Investigation of the microbiology in fluid mud of Seaport Emden ('Emden-FM')

Contract no. 3F1910

Final Report

Julia Gebert[1], Fiorenza Deon[1], Ahmad Shakeel[2], Alex Kirichek[3], Mirjam Perner[4], Stefanie Böhnke-Brandt[4], Ines Krohn[5], Lutgardis Bergmann[5], Floris van Rees[6], Miguel de Lucas Pardo[6]

February 2023

Consortium Deltares-TU Delft

[1]Section of Geo-Engineering, Department of Geoscience and Engineering, Faculty of Civil Engineering & Geosciences, Delft University of Technology, Stevinweg 1, 2628 CN Delft, the Netherlands

[2]Section of Environmental Fluid Mechanics, Department of Hydraulic Engineering, Faculty of Civil Engineering & Geosciences, Delft University of Technology, Stevinweg 1, 2628 CN Delft, the Netherlands

[3]Section of Rivers, Ports, Waterways and Dredging Engineering, Department of Hydraulic Engineering, Faculty of Civil Engineering & Geosciences, Delft University of Technology, Stevinweg 1, 2628 CN Delft, the Netherlands

[6]Deltares, P.O. Box 177, 2600 MH Delft, the Netherlands

Subcontractors

[4]GEOMAR Helmholtz Centre for Ocean Research Kiel

[5]University of Hamburg

Leading author	Deltares co-author	External reviewer	Approver manager
Julia Gebert	Miguel de Lucas	Thijs van Kessel	Laura Vonhögen-Peeters

Contact

Dr. habil. Julia Gebert, Associate professor
T   +31 15 278 2798
E   j.gebert@tudelft.nl

Photo on title page: MS Delphin in Port of Emden

Abstract

Maintenance of the nautical depth in the seaport of Emden, Germany, is achieved by re-circulation of fluid mud using a trailing suction hopper dredger. Continued re-circulation has proven to maintain low settling rates and to keep yield stresses of re-circulated fluid mud below 50-100 Pa, in combination with densities of 1.15-1.2 t/m³ enabling safe navigation through these fluid mud layers. Over the past 30 years, it has been assumed that low-density extracellular polymeric substances (EPS), produced by a highly adapted microbial community, were responsible for the desired effect of keeping fine-grained sediment in suspension and that the regular contact with the oxygenated water phase during re-circulation dredging supports thriving of this microbial community. Climate change models have indicated increased future discharge of fresh water from the hinterland into the saline Port of Emden. It was hypothesized that increased freshwater discharge might alter the composition and activity of the microbial community and hence change the prerequisites for maintaining the currently favourable properties of fluid mud. To investigate these effects, a field study investigating the variability of fluid mud properties and environmental conditions, and a laboratory study, investigating the effects of different levels of admixture of freshwater were carried out. Results suggest that the low yield stresses of fluid mud in the Port of Emden are not the effect of a specialized microbial community producing high concentrations of EPS, but can be solely attributed to a reduction of density of fluid mud as achieved by the current re-circulation practice. More consolidated, denser sediment layers attain similar properties after being re-suspended to lower densities. EPS concentration and composition as well as the degradability of organic matter in fluid mud were subject to pronounced seasonality. The microbial community is highly diverse and responds swiftly to variations in environmental boundary conditions. Further, it appears that future possible increases in the share of freshwater do not affect the sediment's rheological response, settling behaviour and concentration of extracellular polymeric substances and will hence not adversely impact the current dredging strategies for maintaining the nautical depth.

Table of contents

List of figures

List of tables

1   Background and research questions

Maintenance of the nautical depth in the seaport of Emden, Germany, is achieved by re-circulation of fluid mud using a trailing suction hopper dredger (TSHD). Re-circulation dredging results in a material that exhibits low settling rates and low yield stresses of < 50-100 Pa, in combination with densities of 1.15-1.2 t/m³, enabling safe navigation and manoeuvring. Wurpts and Torn (2005) hypothesized that low-density extracellular polymeric substances (EPS), produced by a specific microbial community adapted to the environmental conditions created by re-circulation dredging, were responsible for the desired effect of keeping the fine-grained sediment in suspension. It was further suggested that re-circulation dredging enhanced the contact of suspended sediment with the oxygenated water phase, supporting the thriving of this microbial community.

Climate change models have indicated increased future discharge of fresh water from the hinterland into the saline water of the Port of Emden for the winter months (Figure 1, Spiekerman et al., 2018), affecting the present seasonal patterns of water salinity and composition.
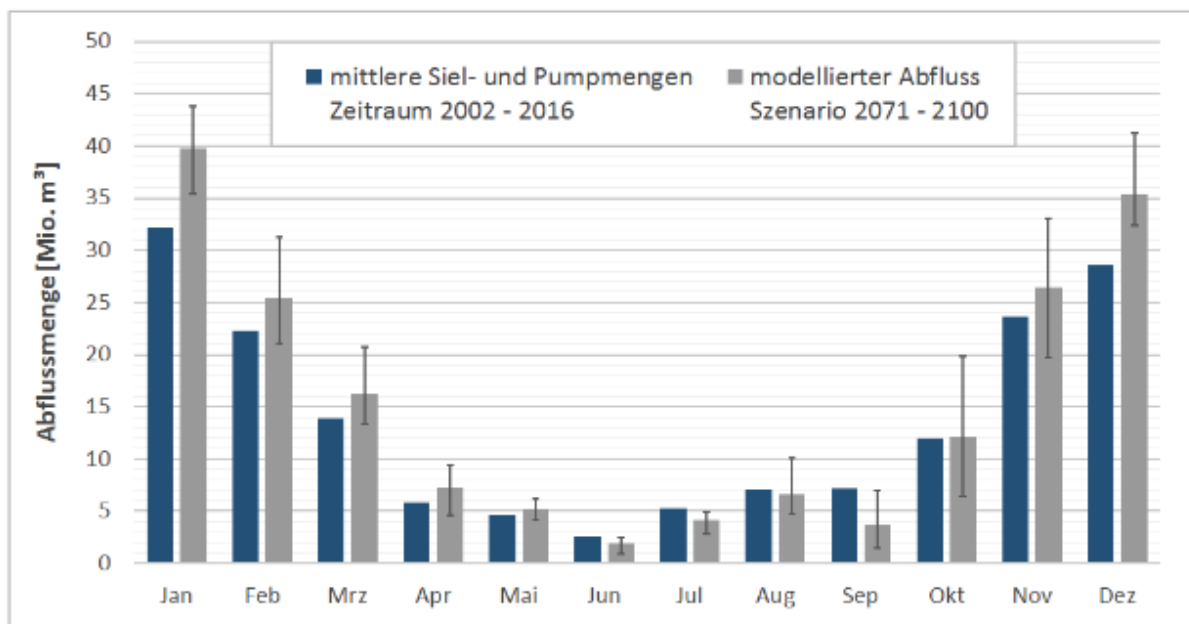
Figure 1. Model based estimation of the seasonal freshwater discharge in the area of the I. Entwässerungsverband due to climate change. Blue: Average of pumped discharge 2002-2016. Grey: average of modelled discharge for different climate scenarios 2071-2100. From Spiekermann et al. (2018).

Microbial activity is closely connected to the availability of degradable organic matter. Settling and rheological behaviour of suspended sediments are related to salinity and to organo-mineral interactions (Deng et al., 2019; Mietta et al., 2009). To anticipate possible effects of increased freshwater discharge on fluid mud properties and hence maintenance of the nautical depth, it was proposed to investigate the effects of

(1) the natural seasonal variability in salinity in the Port of Emden and
(2) changes in the volume ratio of freshwater to saline water

on rheological properties and settling behaviour of fluid mud, and the composition and activity of the microbial community.

A field monitoring program and laboratory experiments were conducted for studying the effect of changes in freshwater discharge on fluid mud properties. Monthly field sampling events were performed in two frequently maintained areas of the Port of Emden (Grosse Seeschleuse and Wendekreis Industriehafen, see Figure 2). Furthermore, laboratory mesocosm experiments with varying volume ratio of saline and fresh water in fluid mud were carried out. It was hypothesized that increased volumetric shares of freshwater might alter the composition and activity of the microbial community, and hence change the boundary conditions for the favourable properties of fluid mud and the current port maintenance strategy in the Port of Emden.

2 Approach

2.1 Field study

Monthly sampling campaigns were conducted between March 2021 and April 2022 at two sites within the Port of Emden, which are shown as GS (Große Seeschleuse) and IH (Industriehafen) in Figure 2 (the left panel). During each of the 12 surveys, the sediment samples were collected from the fluid mud layer that was identified by the dual frequency (200 kHz and 15 kHz) echo sounder. Typically, the fluid mud layer was mapped between ~9 m and ~12 m below the water surface in both locations. The right panel of Figure 2 shows a Beeker sampler that was used for collecting 3 subsamples from the top, the middle and the bottom of the FM layer at each location. and the subsamples were mixed together for obtaining one homogeneous sample per site. On some dates, additional samples were taken to carry out targeted laboratory experiments. These are not included in the list of the regular samples taken for the field study (Table 1).
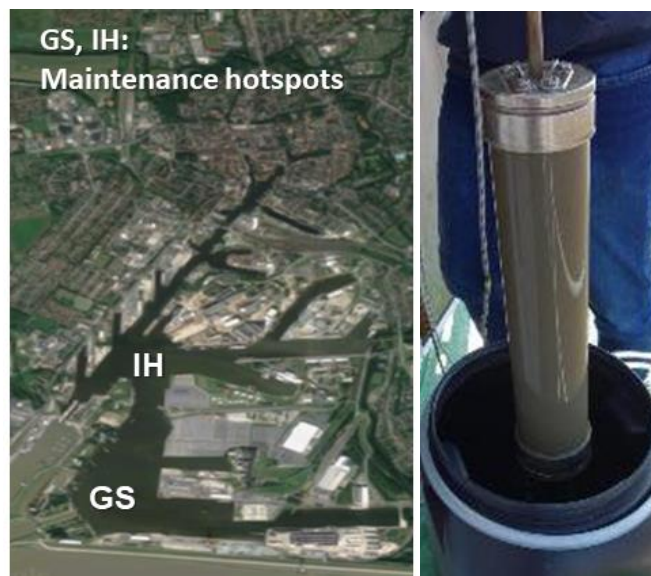
Figure 2. Left: Aerial view on the Port of Emden with sampling locations IH and GS (Source: Google maps). Right: Beeker sampler with fluid mud.

Table 1. Dates of field sampling campaigns, locations and sample numbers of FM samples.

Date	Sample ID	Location	Sample type	Date	Sample ID	Location	Sample type
24.03.2021	1001	GS	FM	28.09.2021	1025	IH	FM
24.03.2021	1003	IH	FM	28.09.2021	1026	GS	FM
21.04.2021	1008	IH	FM	02.11.2021	1027	IH	FM
21.04.2021	1009	GS	FM	02.11.2021	1028	GS	FM
27.05.2021	1010	IH	FM	07.12.2021	1029	IH	FM
27.05.2021	1011	GS	FM	07.12.2021	1030	GS	FM
24.06.2021	1012	IH	FM	20.12.2021	1031	IH	FM
24.06.2021	1013	GS	FM	20.12.2022	1032	GS	FM
20.07.2021	1017	IH	FM	21.02.2022	1033	IH	FM
20.07.2021	1018	GS	FM	21.02.2022	1034	GS	FM
31.08.2021	1023	IH	FM	04.04.2022	1035	IH	FM
31.08.2021	1024	GS	FM	04.04.2022	1038	GS	FM

The mixed samples were subdivided into six aliquots for the following analyses:

1) Composition, activity and cell count of microbial community
2) Concentration and composition of EPS ('slimes')
3) Degradability/stability of organic matter
4) Rheological properties and settling
5) Basic properties: pH, EC, redox potential, density, water content
6) Standard sediment properties (CUA Emden).

Samples were transported to the respective laboratory cooled or, in case of samples designated for transcriptome analysis, on dry ice. Samples for analysis of microbial community composition were fixed using 4 % formaldehyde.

Figure 3. Examples of direct measurements of fluid mud properties. Left: Redox potential of sample 1003 (IH). Right: Visual observation of fluid mud samples. Brownish discoloration is typical for more oxidized fluid mud from GS (sample 1001) and grey colours indicate more reduced oxygen in fluid mud from IH (sample 1003).

2.2 Laboratory experiment

Figure 4 shows preparation of fluid mud mixtures with different salinity, shear rates, sampling and analyses. The fluid mud sampled from location GS in March 2021 (sample 1001, pH = 7.6, electrical conductivity = 8.01 mS/cm) was mixed with fresh water from the Ems-Jade-Kanal (pH 7.6, electrical conductivity = 0.6 mS/cm). Partial substitution of the saline water of the original sample 1001 was carried out in steps from 0 to 50% (see Table 2) to achieve a salinity gradient. After admixing the freshwater and allowing the suspension to settle overnight, the original sediment density (1.08 g/cm^3) was reproduced by removing the appropriate volume of supernatant water. An unsubstituted sample (0%) served as control.

Table 2. Steps of substitution of original water with fresh water from the Ems-Jade-Kanal.

Sample ID	Substitution (% volume of total sample)
0	0
1	10
2	20
3	30
4	50

The fluid mud mixtures were kept in the laboratory at 20 °C between March and November 2021 and sheared weekly for two hours by a 80 mm vane at 320-470 rounds per minute (RPM). The

rotational speed was adjusted to ensure movement of the complete fluid mud volume. At six moments in time (t0, t1, t2, t3, t4, t5; Table 3), subsamples were collected from each previously homogenised mixture and divided into five aliquots for analysing the parameters shown in Figure 4. The conducted analyses were identical to the one listed in section 2.1 for the field monitoring program, with the exception of standard sediment properties that were already determined on the original sample 1001.

Table 3. Dates of subsampling fluid mud at different levels of fresh water substitutions.

Time point	Date	Time point	Date
t0	26.03.2021	t3	25.05.2021
t1	14.04.2021	t4	19.07.2021
t2	29.04.2021	t5	19.11.2021
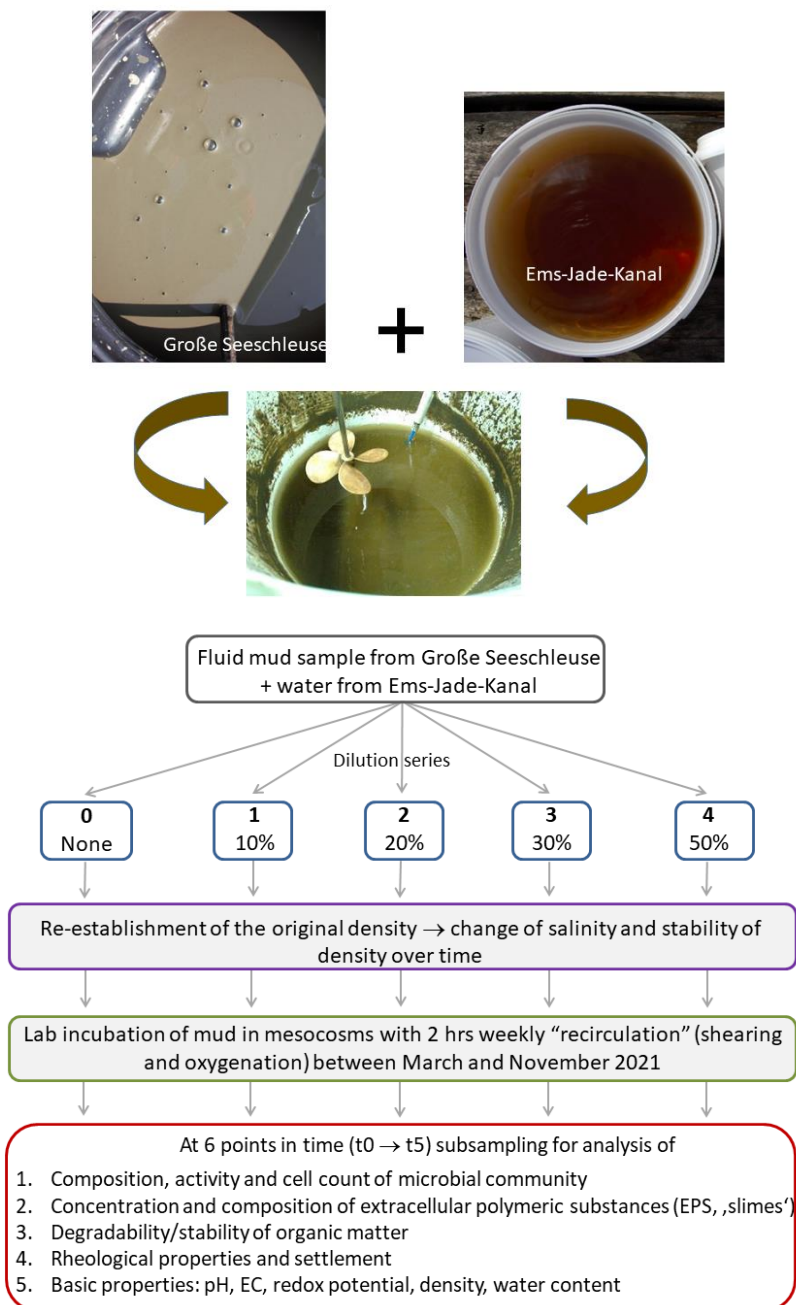
Figure 4. Preparation of fluid mud mixtures of different salinity, shear rates, sampling and analyses.

3 Methods

3.1 Composition, activity and cell count of the microbial community

3.1.1 DNA extraction and 16S metagenomic library preparation

For studying the composition of the microbial community, a 16S metagenomic amplicon library compatible with the Illumina MiSeq System was prepared (Gonnella et al., 2016; Böhnke et al., 2019; Adam et al., 2020; Hansen et al., 2022). DNA was first extracted from around 300 mg sample using the NucleoSpin DNA Soil Mini kit (7.4 and 186 ng µl-1 with a 260/280 nm ratio ranging from 1.76 to 1.87) according to the specifications of the manufacturer (Macherey-Nagel, Düren, Germany). The metagenomic DNA was then used as a template (12.5 ng) for the amplification of (i) the 16S bacterial hypervariable V3/V4 regions using the primer pair S-D-Bac-0341-b-S-17 and S-D-Bac-0785-a-A-21 (Klindworth et al., 2013) and (ii) the 16S archaeal hypervariable V4/V5 regions using the two primer pairs Arch_519F / Arch 915R, (Ding et al., 2017) and Arch 524F / Arch 958R (Cerqueira et al., 2017), respectively. Duplicate PCR reactions were performed for each of the three primer sets (total of 3x2 PCRs per sample) using Kapa Hifi HotStart Ready Mix (Kapa Biosystems, Boston, MA, USA) according to the instructions in the manufacturer's protocol. PCR conditions were set as follows: 3 min initial denaturation followed by 25 cycles of denaturation at 95°C for 30 s, annealing at 55°C and 63°C for amplification of the bacterial and the archaeal 16S rRNA gene, respectively, and extension at 72°C for 30 s. After the pooled bacterial (1x2) and archaeal (2x2) 16S rDNA gene amplifications were purified using the Agencourt AMPure XP Reagent (Beckman Coulter, Brea, CA, USA) multiplexing indices and Illumina® sequencing adapters were added by using the Nextera® XT Index Kit (Illumina) and the Kapa Hifi HotStart Ready Mix (Kapa Biosystems) under the same PCR conditions mentioned above, but with 8 cycles. The quality of bead-based purified (AMPure XP), indexed samples was then verified on the 2100 Bioanalyzer (Agilent Technologies, using the DNA High Sensitivity Chip). The 16S rDNA metagenomic library was sequenced by paired-end sequencing in a 2x300 bp run on the Illumina MiSeq platform (Illumina, St. Diego, USA).

3.1.2 QIME, R, visualization

Sequences were processed using the Qiime2 environment (Bolyen et al., 2019). The filtering and merging of demultiplexed raw reads were performed using the dada2-plugin with default settings and removal of the primer sequences (Callahan et al., 2016). For taxonomic assignments the SILVA database release 138 (Quast et al., 2013) was pre-trained with the respective primer pairs for Bacteria and Archaea (Pedregosa et al., 2011; Kaehler et al., 2019). The assignments were computed using the feature-classifier plugin (classify sklearn) with default settings and the pre-trained SILVA classifier (Kaehler et al., 2019). The phylogeny was calculated using the "align-to-tree-maffft-fasttree" pipeline and alpha diversity (Shannon indices) were calculated with the qiime diversity plugin using a sampling depth of 9019 for Bacteria and 4043 for Archaea (Price et al., 2010). Principle Coordinate Analysis (PCoA) based on weighted and unweighted UniFrac distances and MANOVA to calculate the significance of the differences in the weighted and unweighted UniFrac distances, between the different sampling locations, time points, and layers were performed in R (https://www.R-project.org) using the microeco package (Liu et al., 2021).

Rarefacation for PCoA analyses was performed with different subsample sizes with individual sample sizes of 7000 for Bacteria and 3800 for Archaea.

3.1.3 Real time quantitative PCR (qPCR)

The relative abundances of bacteria and archaea were determined as previously published by Böhnke and Perner (2017), but with the following modifications: A total of 20 ng of the isolated metagenomic DNA was used as a template for amplifying the hypervariable V3/V4 regions of the bacterial and the hypervariable V4/V5 regions of archaeal 16S rRNA gene. Therefor the same primer pairs that have been used for Illumina® sequencing were used, but for qPCR the Illumina® adaptor overhang nucleotide sequence was removed. The SYBR® Select Master Mix, CFX (Applied Biosystems® by Life TechnologiesTM) was used to set up the qPCR reaction. The amplification was performed with the CFX96TM Real-Time System C1000 Touch Thermal Cycler (Bio-Rad, Hercules, CA, USA) under the following conditions: 95°C for 2 minutes followed by 40 cycles of 98°C for 15 seconds, 59°C for 20 second, and 72°C for 30 seconds. Five technical replicates were measured and used to calculate relative quantitative abundances. Next to the samples a non-template control, a non-reverse transcriptase control and a positive control was set up.

3.1.4 Total cell counts

Total cell counts were determined using diamidino-2-phenylindole (DAPI). For this purpose, the mud samples were fixed on board in 4 % formaldehyde/PBS and incubated at 4°C overnight. After washing the cells twice with PBS buffer, they were stored at -20°C in PBS/EtOH [1:1] until further processing. Cells were separated from the sediment by ultrasonication (2 times: 20%, 20 cycles, 20 seconds) then diluted in sterile PBS [1:4000], before being fixed by vacuum filtration (-200 mbar) on 0.2 µm polycarbonate filters. The filters were embedded in low melting point agarose (0.2%, Biozym, Hessisch Oldendorf, Germany) and dried at 37°C for 30 minutes. A section of the filter was cut out, stained with DAPI (10 minutes at room temperature), and embedded in Citifluor prior to counting the cells using a Zeiss Axio Imager.M2 epifluorescence microscope, equipped with a DAPI filter set (Carl Zeiss AG, Oberkochen, Germany).

3.2 Extracellular polymeric substances (EPS)

All analyses were performed in triplicate. 0.14 M NaCl was used as negative control in triplicate. All reactions were measured three times. For the determination of proteins, carbon hydrates and uronic acids standard curves were established by performing the respective assay on dilution series of a standard solution of known concentration in triplicates.

3.2.1 Isolation of EPS

Total EPS was isolated according to Wingender et al. (2001) with a few modifications. Mud samples were weighed and suspended in sterile 0.14 M NaCl solution (mass ratio of sample wet weight to NaCl solution of 1:16, for samples 19201 to 21206 of 1:10). The mud suspensions were stirred on a magnetic stirrer for 60 min with 200 rpm at room temperature. To remove unsolved particles the suspensions were centrifuged for 30 min at 20,000 x g at 10 °C. The decanted

supernatants were filtered two times through cellulose acetate membranes (pore diameter, 0.2 µm). Aliquots were stored at -20 °C.

3.2.2 Extraction of DNA

200 µL of isolated EPS solution were used for extraction of DNA by Monarch® PCR & DNA Cleanup Kit (NEB #T1030) according to the manufacturer's instructions. DNA was eluted with 20 µL of nuclease-free water, heated to 60 °C. To increase the DNA yield the eluate was pipetted onto the matrix again and eluted a second time. DNA concentration was measured with Nano-Photometer® NP80 (Implen GmbH).

3.2.3 Analysis of proteins

Determination of proteins was performed according to Frølund et al. (1996), a modification of Lowry et al. (1951). 700 µL of Lowry reagent were added to 500 µL of isolated EPS solution and mixed by vortexing. After 10 min of incubation at room temperature, 100 µL of Folin-Ciocalteus-Phenol reagent solution was added and immediately mixed by pipetting. After 45 min of incubation at room temperature in the dark absorption was measured at 750 nm with NanoPhotometer® NP80.

The Lowry reagent was composed as follows:

Solution 1: 0.143 M sodium hydroxide and 0.270 M sodium carbonate were dissolved in 500 mL of ddH$_2$O.

Solution 2: 0.057 M copper sulphate was dissolved in 10 mL of ddH$_2$O.
Solution 3: 0.124 M sodium tartrate dihydrate was dissolved in 10 mL of ddH$_2$O.
Solutions 1, 2 and 3 were mixed in the volume ratio of 100:1:1.
Folin-Ciocalteus-Phenol reagent and ddH$_2$O were mixed in a volume ratio of 0.83:1.

3.2.4 Analysis of carbohydrates

Determination of carbon hydrates was performed according to Dubois et al. (1956). 500 µL of 5% (w/v) phenol solution and 2.5 mL of 100% sulfuric acid were added to 500 µL of isolated EPS solution most quickly and mixed by vortexing. 10 min of incubation at room temperature were followed by 15 min of incubation at 30 °C in a water bath and another 5 min of incubation at room temperature in the dark. Absorption was measured at 480 nm for acidic polysaccharides and 490 nm for neutral polysaccharides with NanoPhotometer® NP80.

3.2.5 Analysis of uronic acids

Determination of uronic acids was performed according to Filisetti-Cozzi & Carpita (1991). 80 µL of solution 1 and 2.36 mL of solution 2 were added to 400 µL of isolated EPS solution and mixed by vortexing. 20 min of incubation at 100 °C were followed by 5 min of incubation in an ice bath. After addition of 80 µL of solution 3 and mixing by vortexing the reactions were incubated for 10 min at room temperature in the dark. Absorption was measured at 525 nm with NanoPhotometer® NP80.

Solution 1: 2 M amidosulfonic acid.
Solution 2: 0.075 M sodium tetraborate decahydrate in sulfuric acid.
Solution 3: 0.15% (w/v) 2-phenylphenol in 0.5% (w/v) sodium hydroxide solution.

3.2.6 Analysis of lipids

Determination of lipids was performed according to Hara & Radin (1978) with few modifications. 500 µL of n-hexane were added to 500 µL of isolated EPS solution and homogenized by rigorously vortexing on a vortex-genie® 2 (Scientific Industries) with adapter for 24 samples for 30 min at room temperature. After a centrifugation step at 12,000 x g for 90 sec at room temperature 400 µL of the upper phase were pipetted into a previously weighed test tube avoiding the interphase. After 24 h of drying the test tube was weighed again and the lipid mass was determined by subtracting the weight of the empty test tube.

3.3 Anaerobic degradation of organic matter: Gas generation

200 g of fresh sample were placed in triplicates into 500 ml glass bottles. The bottle headspace was flushed with 100% N_2 to establish anaerobic conditions and incubated at 36 ˚C in dark. Gas production over time was quantified through the increase in pressure within the bottle headspace. At dedicated time intervals, gas composition was determine using a gas chromatograph. Gas generation was calculated according to the ideal gas law using the gas concentration, the headspace volume, the incubation temperature, and the pressure inside the bottle. The share of dissolved gas in water (mainly CO_2) was assessed using Henry's law based on the CO_2 concentration and the pressure as well as the solubility of CO_2 in water as given by Henry's constant (listed in Sander 2015). The total amount of generated gas equals the sum of CO_2 and CH_4 produced and was expressed as mass unit of carbon released per mass unit of organic carbon (as present in the original sample) and per mass dry weight.

3.4 Aerobic decay of organic matter: Respiration

To determine the degradation of organic matter under aerobic conditions, 15 g of homogenised fresh sample were incubated in 1 l glass bottles at 20 ˚C in dark. To avoid the degradation of organic matter to be limited by elevated CO_2 concentrations, the bottle headspace was flushed with synthetic air after CO_2 concentrations had reached 3% in the gas phase, then measurements were resumed. The amount of degraded carbon was calculated using the concentration of CO_2 as measured by gas chromatographic analysis and the bottle headspace. Respiratory C-release was related to mass unit organic carbon present in the sample at the beginning of the incubation and to mass dry weight.

3.5 Particle size distribution, density and settling

Analysis of the **particle size distribution (PSD)** of fluid mud in the range of ≤ 2µm (clay) to 2000 µm (equivalent to coarse sand) was conducted using static light scattering (Malvern MasterSizer 2000MU). Organic matter or any other bonding agents were not destroyed before the analysis, so that the data reflect the sizes of any assemblages formed by, for example, flocculation. The diameter of particles is estimated as a volumetric share (%). Fluid mud **density** was determined by Anton Paar density meter (DMA 35).

The **settling properties of fluid mud** were estimated by tracing the mud-water interface over time in Hirschmann 1000:10 mL settling columns within 24 hours (see Figure 5, left), during which the height change was always linear over time (Example given in Figure 5, right). Prior to the start of the test, the fluid mud was homogenized manually with a metal spoon for 2 minutes. Subsequently, the settling column was filled with 1000 mL of the homogenized mixture and sealed with plastic film to limit evaporation. The settling columns were photographed every 600 seconds with a Canon EOS 500D camera with LED-backlight placed behind the columns to foster contrast between water and mud. Standard Canon control software, EOS Utility, was used to control the intervals of taking photos.

The mud-water interface was tracked by analyzing the taken photos using two methods: 1) manual tracking the interface through the photos and 2) with an automatic interface-extraction script. Manual tracking the water-mud interface was performed by recording time and mud volume at the moment the water-mud interface crossed a new 10 mL increment. Volume was converted into height. The slope of the trend line of the interface height versus time is equivalent to the settling velocity. The automatic image extraction method was used to elucidate the non-linear part of the height versus time plot, because a longer timeframe (>24 h) could be processed with 600 s time intervals. This was executed to verify if linear regression could be used for slope estimations. This method was not used to compute the settling rates because it fails for the photos taken at the start of the test. This script was able to acquire the vertical pixel location at which the maximum gradient in pixel values is present. Lighter pixels and darker pixels have high pixel values and low pixel values, respectively. The maximum gradient location was assumed to be the water-mud interface. This pixel location was converted to height using control points in the photo.

Reproducibility of settling rate data was verified by conducting a settling column experiment in triplicates on the same sample. The deviation in settling rate between the triplicates was less than 5%.
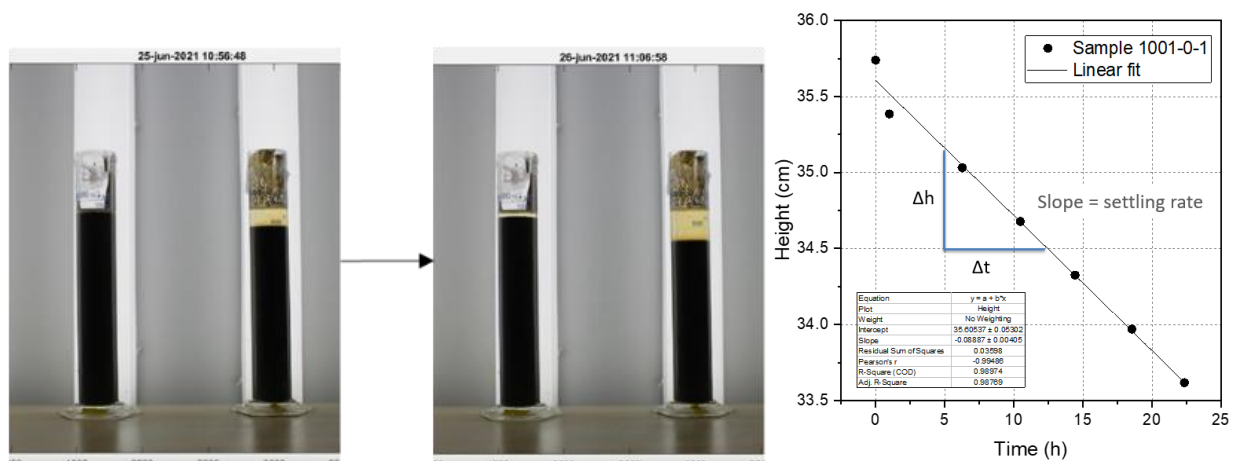
Figure 5. Left: Settling column setup. Right: Estimation of settling rates by example of sample 1001-0-1 Settling rates were calculated based on the slope of the linear trend line within the first 24 hours.

3.6 Rheological analyses

The rheological analysis of mud samples was performed using a HAAKE MARS I rheometer (Thermo Scientific, Karlsruhe, Germany) with Couette geometry (gap width = 1 mm). The mud samples were gently homogenized before each experiment. After placing the bob into the cup with mud sample, a waiting time of 30-50 s was adopted, in order to minimize the disturbances created by the bob. The rheological experiments were performed at 20 °C, maintained by a Peltier controller system. In order to check the repeatability, all the experiments were performed in duplicates .The estimated repeatability error was less than 2%. In order to estimate the yield stress of the mud samples, stress ramp-up tests were performed by linearly increasing the stress at a rate of 0.1 Pa s^{-1}, until the shear rate reaches 300 s^{-1}. The corresponding rotation of the geometry was measured, which eventually provided the shear rate and the apparent viscosity. The outcome of the test was plotted in terms of the apparent viscosity as a function of the shear stress. Following the protocol of Shakeel et al. (2020), the static yield stress (SYS) and fluidic yield stress (FYS) were determined.

3.7 Standard sediment properties

Standard solids and pore water properties, and components were analysed by the protocols listed in Table 4, provided by the Chemisches Untersuchungsamt Emden (CUA).

Table 4. Protocols for analysing standard properties of solids and pore water. Source: Chemisches Untersuchungsamt Emden (CUA).

Parameter	Method	Parameter	Method
Dry mass	DIN 19747:2009-07	DOC	DIN EN 1484 (H3): 2019-04
Loss on ignition	DIN EN 14346:2007-03	NH$_4$	DIN 38406-5:1983-10
TOC	DIN EN 15936: 2012-11	NO$_2$	DIN EN 26777 (D10): 1993-04
TN	DIN EN ISO 13878:1998-11	NO$_3$	DIN 38405-9:2011-09
pH	DIN EN ISO 10523 (C5): 2009-07	Fe, Ca, Li, Al. Mn, Vn, Na, K, Si, P	DIN EN ISO 17294-2 (E29): 2017-01
EC	DIN EN 2788 (C8): 1993-11	S	DIN EN ISO 10304-1 (D20): 2009-07
O$_2$ consumption	DIN V 38408-24: 198-08		

TOC = total organic carbon   TN = total nitrogen
EC = electrical conductivity   DOC = dissolved organic carbon

3.8 Targeted laboratory experiments

In order to verify the relationships between density, yield stresses and settling rates found for the monthly field samples, targeted laboratory experiments were carried out using additional field samples.

3.8.1 Effect of substituting saline with fresh water, field sample

In analogy to the laboratory experiment described in 2.2, a dilution series (10%, 20%, 30% and 50%) was carried out on fluid mud sample 1024 collected at site GS in June 2021, using fresh water from the Ems-Jade-Kanal. After admixture of fresh water, the original density of 1.12 t/m^3 was re-established by withdrawing the corresponding amount of supernatant water. Thereafter, static and fluidic yield stresses were measured.

3.8.2 Effect of diluting fluid mud with in situ water on settling rate and yield stress

To verify the relationship between density and rheological properties observed in the field study, fluid mud from GS (sample 1038) and IH (sample 1035) locations was diluted with water collected in situ to produce four different densities. Subsequently, the settling rates were determined as described in section 3.5.

3.8.3 Effect of diluting consolidated sediment with in situ water

In this experiment, consolidated sediment from the non-maintained sites B, TB, and D (see Figure 6, the left panel) was collected and diluted with in-situ water, thereby adjusting the mud to different densities. Subsequently, the effects of dilution on sediment rheological behaviour were analysed.

Figure 6. Left: Locations B, TB and D. for sampling of consolidated mud. Right: Example of a consolidated mud sample.

4   Results and discussion

This section presents selected properties of the sediment sampled in the Port of Emden, partially in comparison to data from the BIOMUD library for the fluid mud from the Port of Hamburg. The data are grouped according to physical, chemical and biological properties. The dataset for this study is presented in the Excel file that is attached to the report.

4.1   Field study

4.1.1   Physical properties of fluid mud

4.1.1.1   Particle size distribution (PSD)

Both sites were characterized by a very similar particle size distribution, dominated by the fraction < 63 µm which was also more or less constant over time (Figure 7, Figure 8). The highest share of the particles can be attributed to the size equivalent to medium silt (6.3 to 20 µm) with a share of 39 to 42 vol% in GS and 36 to 44 vol% in IH, peaking at around 9 µm (see Figure 7, top panel). Two samples from site IH stand out by larger shares of slightly larger particles (see Figure 7, top right panel). The share of the clay-sized particles ranges from 3.6 to 4.9 vol% in for GS and 4.7 to 6.9 vol% for IH. The fine sand ranges from 7.1 to 10.2 vol% in the GS batch and 7.12 to 10 vol% in the IH batch of samples.

The sum of the volumetric particle sizes corresponding to silt and clay was very similar to the gravimetric share of silt and clay analysed for fluid mud of the Port of Hamburg (see Figure 8).
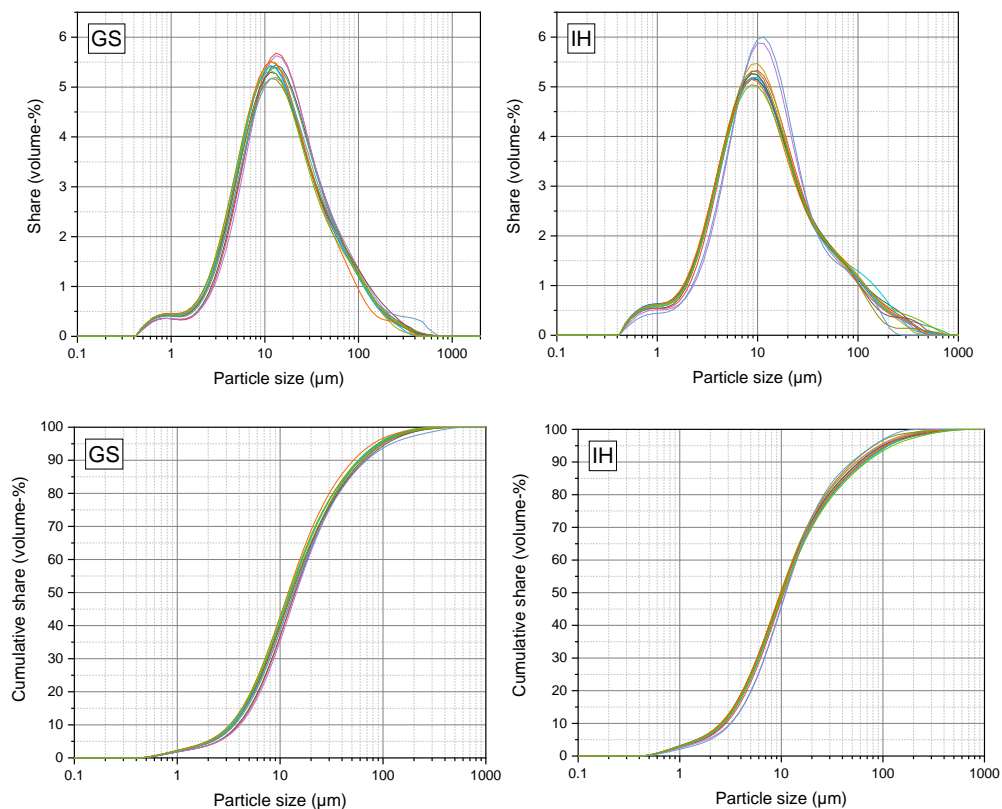
Figure 7. Particle size distribution at site GS (left) and IH (right). Top: Volumetric share of individual particle size ranges, bottom: cumulative curve.
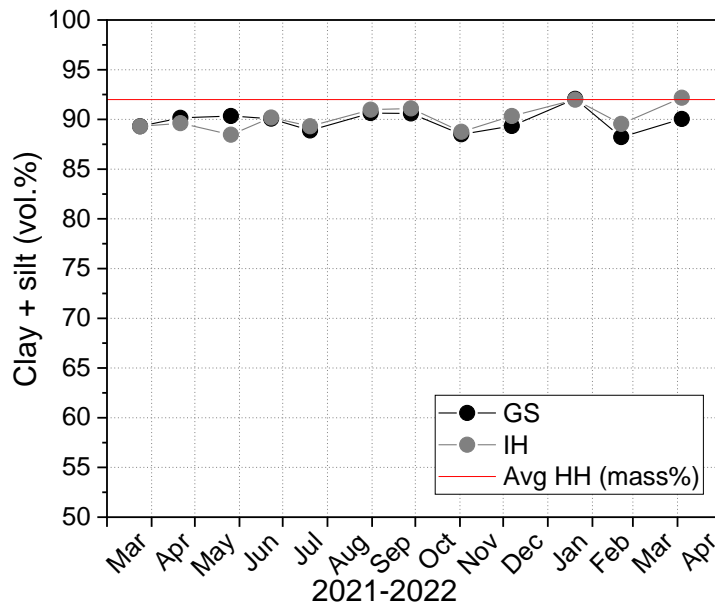
Figure 8. Share of size fraction < 63 μm (sum of clay-sized and silt-sized particles). Red line: Average value for fluid mud in the Port of Hamburg.

4.1.1.2 Dry mass and density**

The **dry mass** for location GS ranges from 11.60 % in April 2021 to 19.3 % in June 2021. For the samples from IH, values from 15 to 20% are observed. Dry mass appears to vary seasonally with higher values in the summer and lower values in spring. A higher value can be observed for the samples collected in IH except in three cases: September, June and December. Overall, the samples from IH show a higher dry mass than those from GS. Samples in the same timeframe, such as in April 2021, February 2022 and April 2022 indicate a difference of up to 5 %-points between the two locations.

Corresponding to the dry mass, the fluid mud at IH had a higher **density** at all points in time, except in September 2021, and also exhibited the same seasonality as the dry mass. Samples from February and April 2022 show a considerable difference in density, with fluid mud from IH showing a higher density of up to 0.04 t/m^3.
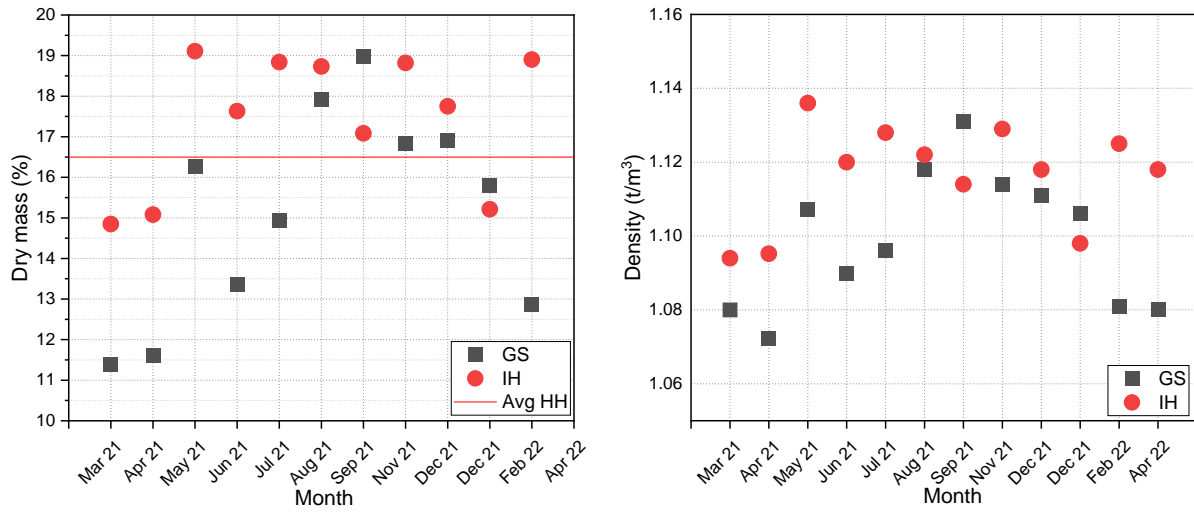
Figure 9. Dry mass (left) and density (right) of fluid mud at GS and IH. Red line: Average value for fluid mud in the Port of Hamburg.

4.1.1.3 Yield stress

Fluid mud from the Port of Emden had very low yield stresses with values mostly below 3 Pa for the static yield stress (SYS) and below 11 Pa for the fluidic yield stress (FYS), which is in the lower range of values found for fluid mud in the Port of Hamburg (see Figure 10). For most of the measured points in time, the yield stresses at site IH were higher than at site GS. The ratio between FYS and SYS averaged around 3 for both sites, similar to fluid mud from the Port of Hamburg (Shakeel et al., 2020), with more consolidated material mostly showing a higher ratio. SYS and FYS at both sites varied over time, exhibiting a non-linear relation to the density of fluid mud (Figure 11). The observed scattering of yield stresses is assumed to be related to the time that passed between sampling and the most recent events of maintenance.
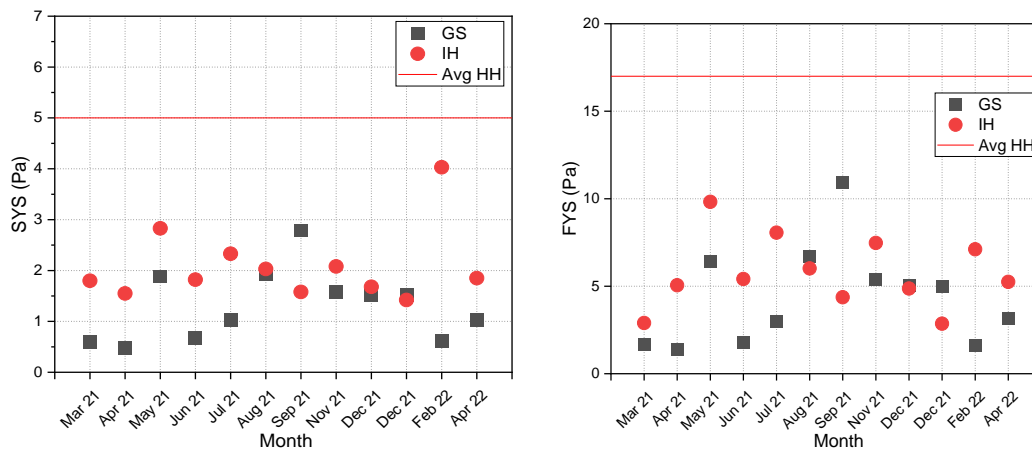
Figure 10. Fluidic (FYS, left) and static (SYS, right) yield stresses. Red line: Average value for fluid mud in the Port of Hamburg.
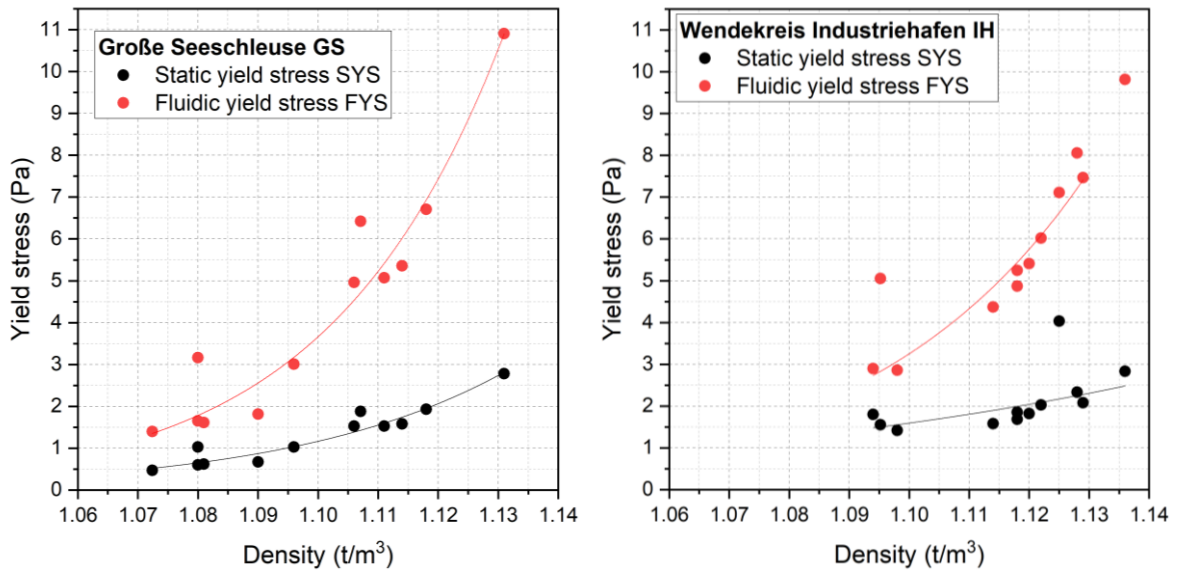
Figure 11. Relationship between fluid mud density and yield stresses at sites GS (left) and IH (right).

4.1.1.4 Settling rate

Most of the settling rates, determined for the initial phase where the lowering of the water-mud interface is linear, ranged below 15 mm/d (Figure 12, left panel). Higher rates were only observed for site GS. As the yield stress, settling rates of fluid mud were strongly density-dependent, however, characterised by a similar inverse relationship for both sites (Figure 12, right panel). The highest settling rates (site GS) were related to the lowest densities whereas conditions of hindered settling or possibly commencing consolidation, were observed at densities >1.09 t/m^3. No systematic impact of the salinity and hence the fraction of fresh water on density, yield stresses or settling rates was observed (Figure 12, right panel).
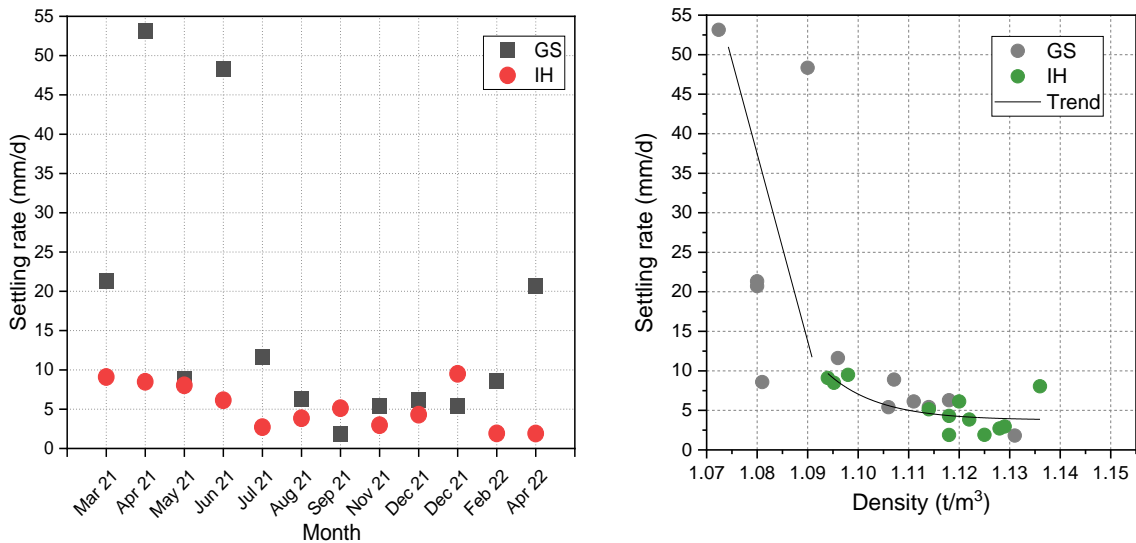
Figure 12. Settling rates over time (left) and in relation to density (right).

4.1.2 Chemical properties of fluid mud

4.1.2.1 Redox potential, pH and salinity

Except for March 2021 at site GS (also see photo in Figure 3, right), all fluid mud samples had negative redox potentials, indicating oxygen-deficient conditions (Figure 13, left panel), albeit slightly less negative than observed in the Port of Hamburg. pH values range around neutral to slightly alkaline with values between 7 and 8 (Figure 13, middle panel). Owing to its near-sea location, salinity and the resulting electrical conductivity (EC) in the Port of Emden are significantly higher than in the freshwater Port of Hamburg. At both sites, salinity exhibited a clear seasonality with increasing values towards summer up to 18 mS/cm (~11.9 ppt) and decreasing values towards winter, with minimum values of around 7 mS/cm (~ 4.3 ppt). Salinity in the inner harbour is driven by the extent of freshwater inflow, which due to elevated evapotranspiration in combination with often reduced precipitation is less in summer than in winter. Higher values at site GS are explained by inflow of saline water from the Eems-Dollard upon opening of the lock. In the investigation period, EC values varied by a factor of 3, by far exceeding the changes predicted for the region by climate change modelling, as reported by Spiekerman et al. (2018, see also Figure 1).
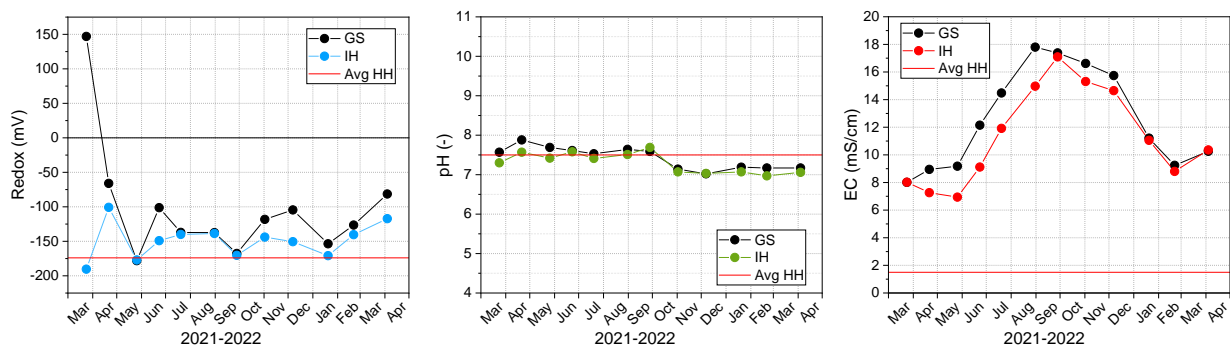
Figure 13. Redox potential (left), pH (middle) and electrical conductivity (EC, right) of fluid mud at sites GS and IH. Red line: Average value for fluid mud in the Port of Hamburg. 1 EC = ~0.6 ppt (parts per thousand).

4.1.2.2 Total organic carbon (TOC) and total nitrogen (TN)

The **TOC** contents (Figure 14, left) ranged between 3.4 and 4.7% of the dry mass and were very similar or both sites, except for March 2021, where a clearly elevated TOC content was found for GS (4.2%, compared to IH, 3.5%). Between April 2021 and December 2021 values remained similar, ranging between 3.5 and 4% for both sites. A considerable increase is detected in the samples of February 2022, where TOC contents at site GS reached up to 4.7%, decreasing again in the last samples collected in April 2022. TOC contents for the Port of Emden are similar to the average values in the Port of Hamburg.

The **TN** values (Figure 14, middle panel) range from 0.2 (IH) in April 2022 to approximately 0.5 % (also IH) in both March and May 2021. With one exception in November 2021, nitrogen contents were similar at both sites. Over time, three peaks were observed, in March, May and November 2021. For the rest of the samples, nitrogen contents remained rather constant between 0.3 and 0.4 %. The results from the last campaign indicate a decrease of the value for both GS and IH to 0.2 to 0.25 % in April 2022, leading to an increased **ratio of TOC to TN** (see Figure 14, right panel). The order of magnitude of the TOC/TN ratio in both cases is very close to values reported

for phytoplankton biomass (Blume et al., 2016; Liefer et al., 2019). No consistent differences between both sites were detected. In relation to the lower TN concentrations, the average TOC/TN ratio of the Port of Emden is higher than the values measured for the Port of Hamburg.
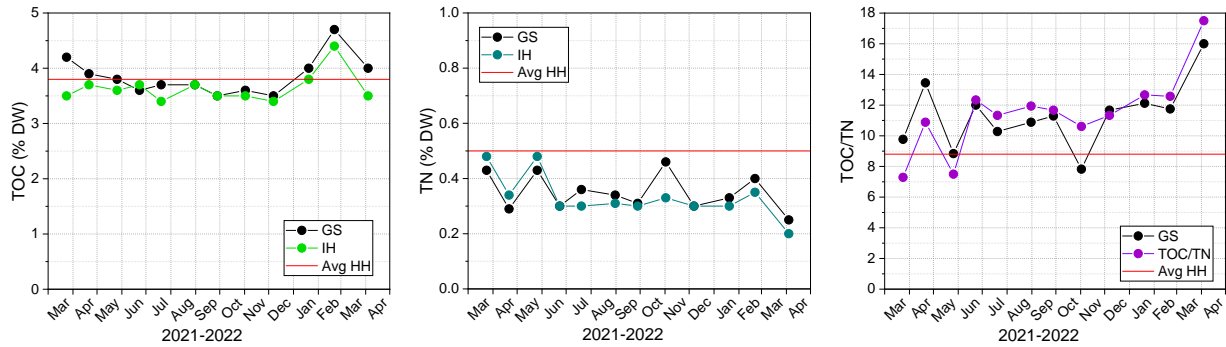
Figure 14. Total organic carbon (TOC, left), total nitrogen (TN, middle) and the resulting TOC/TN ratio (right) in fluid mud at sites GS and IH. Red line: Average value for fluid mud in the Port of Hamburg.

4.1.2.3 Concentration of selected minerals and elements in fluid mud solids

In this section, the concentration of selected characteristic elements for the solid mud from locations GS and IH are shown. The choice of the described elements is based on the mineral composition of the sediments. The sediment samples are characterized by quartz, calcite (Ca) and sheet silicates (Al bearing silicates such as muscovite illite and montmorillonite). Moreover, Fe bearing phases such as chlorite were previously reported (Deon 2021). The qualitative mineral composition (quartz, calcite and sheets silicates) of the sediments from the Port of Emden is similar to the composition of sediments from other ports, such as the Port of Rotterdam and the Port of Antwerp. Some differences are observed in the clay modal composition and in the calcite abundances (see Deon 2021).

Elemental concentrations observed for fluid mud solid samples from the Port of Emden were comparable with sediments along the North sea coast. Dellwig et al. (2000) reported concentrations of approximately 20000 mg Al/kg, 28000 mg Ca /kg and 14000 mg Fe/kg from Helgoland mud sediments. The lowest **Ca** (calcium) concentrations ranged from 15000-19000 mg/kg DW detected for IH and GS in December 2021, respectively, to 63000 mg/kg DW in the sample from IH collected in September 2021 to nearly 80000 mg/kg DW measured in the GS probe from May 2021 (Figure 15). Concentrations differ significantly in May 2021: the Ca concentration in the GS sample was almost twice as high as at site IH 40000 mg/kg DW, likely caused by differences in calcite content. Previous mineralogical analyses on mud samples from the Port of Emden indeed confirmed the occurrence of calcite in considerable abundances (≥ 5 wt. %).

Al (aluminium) concentrations ranged from values around 10000 mg/kg DW in March 2021, December 2021 and April 2022 for both sides IH and GS to a maximum of 48000 (May 2021) for the sample collected in GS. Unexpectedly, the correspondent sample from IH has an Al concentration of 28000 mg/kg DW. These values were re-confirmed by the laboratory in Emden (Chemisches Untersuchungsamt). Al concentrations for GS and IH were mostly very similar and concentrations in the same high range as already analysed and reported by the BIOMUD project for Emden samples (40000-50000 mg/kg DW).

The **Fe** (iron) concentration at both sites was in most cases very similar and significantly exceeded those reported by Dellwig et al. (2000) for North Sea sediment. Samples from GS collected in May and July 2021 showed concentrations of up to 63000 mg/kg DW, far above the other measured values. The Fe concentration reported by Dellwig et al. (2000) only matches the lowest values of approximately 15000 mg/kg DW. The elevated Fe concentrations found in the Port of Emden could be due to Fe import with hinterland water, typically Fe-enriched in the quarternary lowlands of Niedersachsen (NLWKN, 2019), or to an Fe source in relation to port industrial activities.

S (sulphur) concentrations were mostly below 1 mass% for both sites. However, the samples from GS in April 2021 deviate from the series with an S concentration of 6%, most likely caused by the occurrence of pyrite or different sulphur bearing minerals in the sediments. Concentrations of around 3% S were found in the samples from GS gathered in July 2021 and April 2022.

Figure 15. Concentrations of total Ca, Al, Fe and S in fluid mud at sites GS and IH. Red line: Average value for fluid mud in the Port of Hamburg.

4.1.2.4   Concentration of selected elements in fluid mud pore water

From the analyses of the filtrate of pore water **Ca, Fe, Mg, Na, Cl, Mn, NH₄, SiO₂** were selected.

The pore water samples from both sites had similar **Ca** concentrations in all sampling campaigns, with one outlier from GS in November 2021 with a Ca concentration of approximately 300 mg/L,

which is far above the rest of the samples showing concentrations between 100-200 mg/L (Figure 16, left panel). The range of the Ca concentrations is similar to the average Ca concentration from the Port of Hamburg (around 170 mg/L).

The pore water **Fe** concentrations were very low in the first three campaigns (March-May) with an abrupt increase in June for the sample from **GS** and July for the samples from both locations (Figure 16, right panel). The concentrations decreased again in August to a few mg/L. After a gradual increase, the values dropped again for the samples in February and April 2022. For several samples, i.e. June 2021, a remarkable difference in the values between IH and GS was noticed, where IH showed the highest Fe concentration at 16 mg/L. Fe concentrations measured for the Port of Emden partially reflect the average Fe concentration of the Port of Hamburg. However, in many samples this level was exceeded. High Fe pore water concentrations likely originate from the influx of Fe-rich freshwater from the hinterland marsh areas or from specific industrial activities in the port. Fe^{2+} ions facilitate formation of large open flocs and could explain the low settling velocities observed in the field.

Figure 16. Concentrations of total Ca and Fe in fluid mud pore water at sites GS and IH. Red line: Average value for fluid mud in the Port of Hamburg.

The samples from GS and IH had similar concentrations of **Na** (sodium, Figure 17, left panel). Na concentration patterns reflect the prevalence of saline sea water and its variation due to the seasonal variation in freshwater inflow. The highest concentration was measured in November 2021 with 2100 mg/L. Besides one exception, the Na concentrations were much higher than in the fresh water Port of Hamburg, as expected.

The trend for the **Cl** (chloride) concentrations shows a constant increase between March and August and a slower decrease until April 2022 (Figure 17, right panel). Cl concentrations reflect the curve shown for EC and hence indicate the share of saline/fresh water in the port. Similarly to Na, the Cl concentration of the Port of Emden is much higher than in the Port of Hamburg.
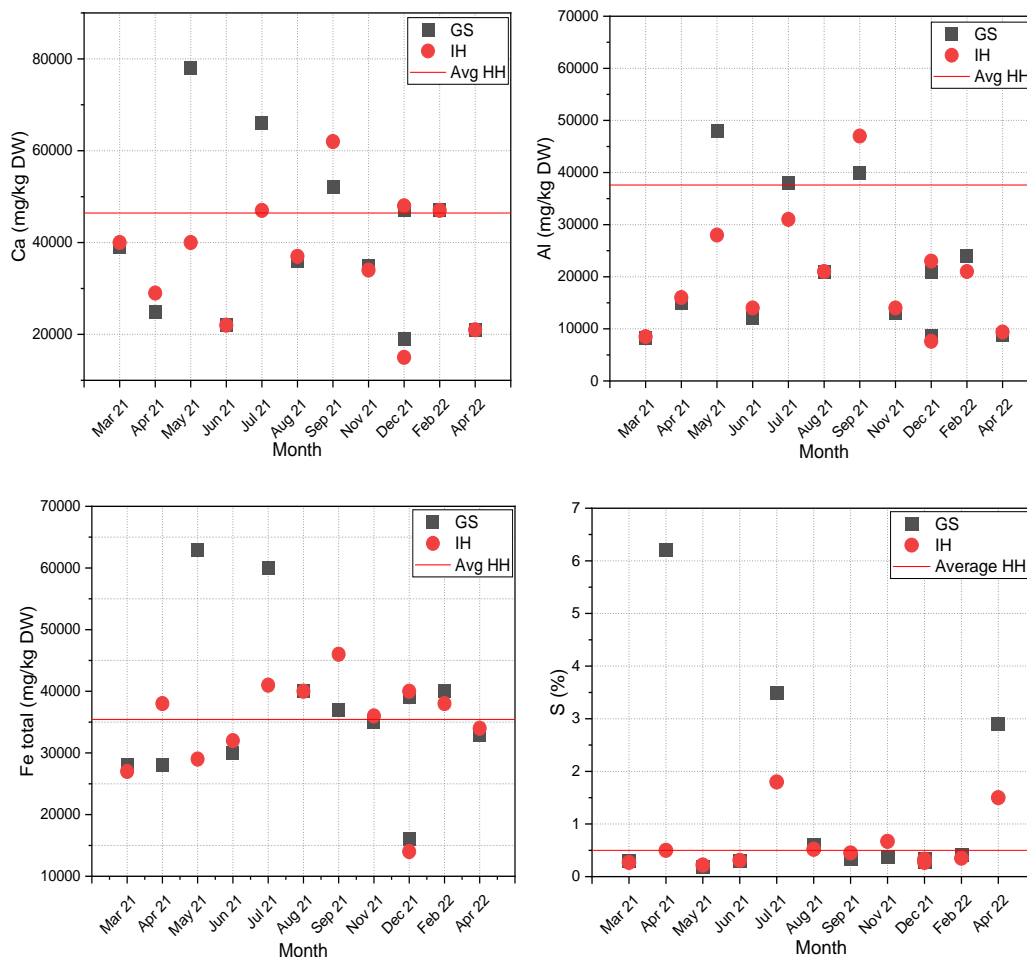
Figure 17. Concentrations of total Na and Cl in fluid mud pore water at sites GS and IH. Red line: Average value for fluid mud in the Port of Hamburg.

NH₄ (ammonium) concentrations in the pore water of fluid mud were quite low. Values varied seasonally with increasing values until September 2021 and a decreased values thereafter. This trend likely reflects the seasonal trend of organic matter degradation. In June, August and September 2021, site GS had higher concentrations, possibly resulting from the influx of fresh organic matter upon opening of the sea lock. The average NH₄ concentration in the Port of Hamburg is much higher than the values measured in the Port of Emden.

SiO₂ is an important mineral for different algal species, especially diatoms (see also Figure 25). In general, the SiO₂ concentration is higher at IH than at GS. The measured values scatter over time from 12 mg/L in April 2022 for GS to 28 mg/L in March 2021 for IH. Concentrations at site IH were consistently higher than at site GS. The average concentration in the Port of Hamburg is within the range of values in the Port of Emden. It is recommended to conduct additional measurements of SiO₂ concentrations in the sediments by means of X-ray fluorescence (XRF) for comparing the concentrations in water and sediment for future investigations.

On average, the **Mg** (magnesium) concentration in pore water samples was similar for both sites. The values decreased from March to August and thereafter increased until November, followed by a steady decrease until April 2022. The observed trend shown by the Mg concentration can be roughly compared to the one of the Na concentration and likely reflect seawater dynamics. Similar to Na, the average Mg concentration for pore water in the Port of Hamburg are far below the values detected in the Port of Emden.
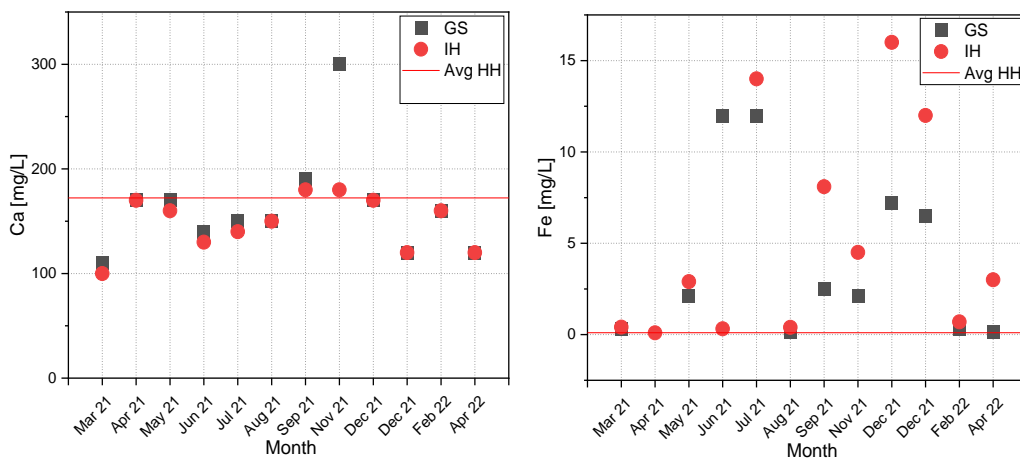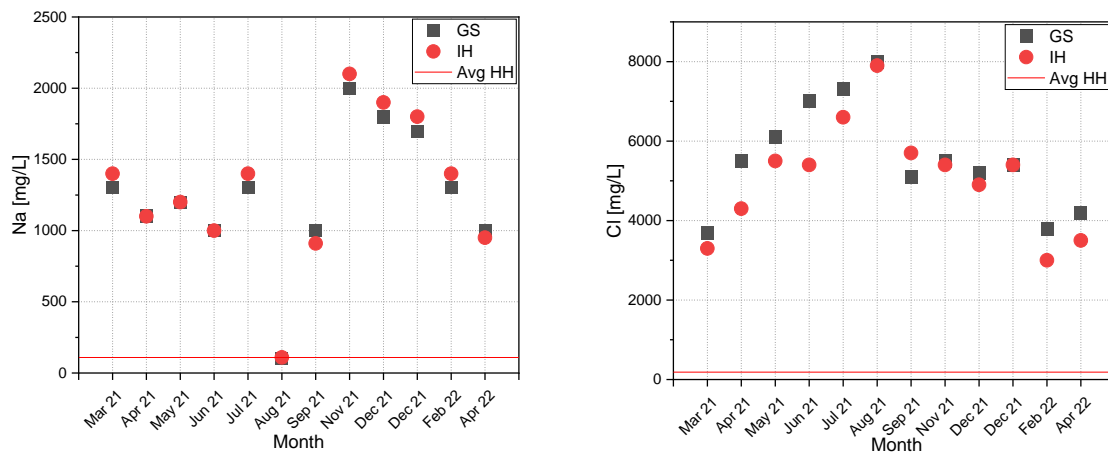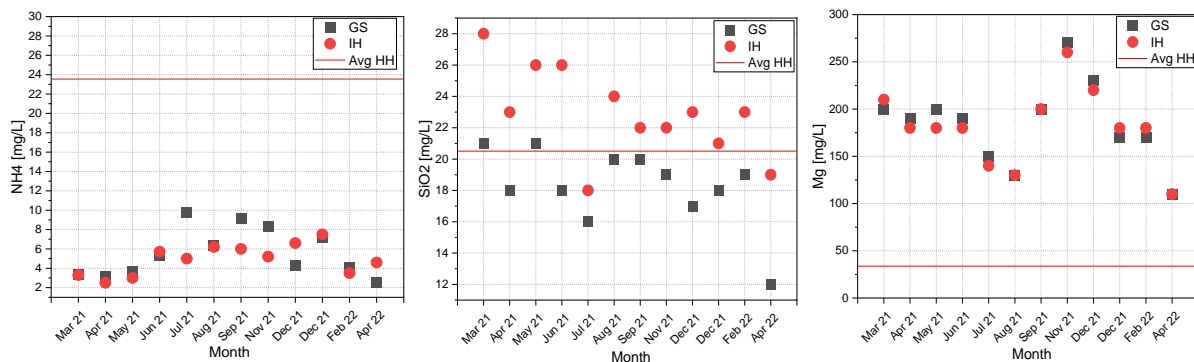

Figure 18. Concentrations of total NH₄⁺, SiO₂ and Mg²⁺ in fluid mud pore water at sites GS and IH. Red line: Average value for fluid mud in the Port of Hamburg.

21

4.1.3 Sediment biological properties

4.1.3.1 Degradation (decay) of organic matter

Microbial decay of fluid mud organic matter was measured as carbon (C) release over time. If C release is normalised to organic carbon (TOC) present in the sediment at the beginning of the analysis, the degradability (lability) of the organic matter can be inferred. Higher C release per unit TOC indicates higher degradability, and a lower C release per unit TOC a lower degrdability of the organic matter.

Organic matter decay varied between sites GS and IH and over time (Figure 19). Absolute release of organic carbon, expressed by the mass of carbon released per unit dry weight (Figure 19, the left panels), but also the degradability of organic carbon, expressed by the mass of carbon released per unit organic carbon (Figure 19, right panels), were typically higher at site GS over the entire investigation period. For both parameters, differences were higher in the first half (until approximately August 2021) and became less pronounced in the second half of the investigation period. Higher organic matter decay rates and higher degradability at site GS, here expressed as the cumulative mass of carbon released in 21 days, could originate from higher input of easily degradable organic matter of phytoplankton origin (Zander et al. 2022) from the Eems-Dollart at site GS through the regular opening of the lock for vessel traffic. As primary production ceases in fall and winter, and the input of fresh, easily degradable organic matter declines, the differences between the two sites become less pronounced at the second half of the investigation period. Fluid mud TOC and TN contents, however, were similar at both sites and do not support this hypothesis, or analytical sensitivity was not high enough to detect small, but relevant differences in TOC and TN contents between the two sites.
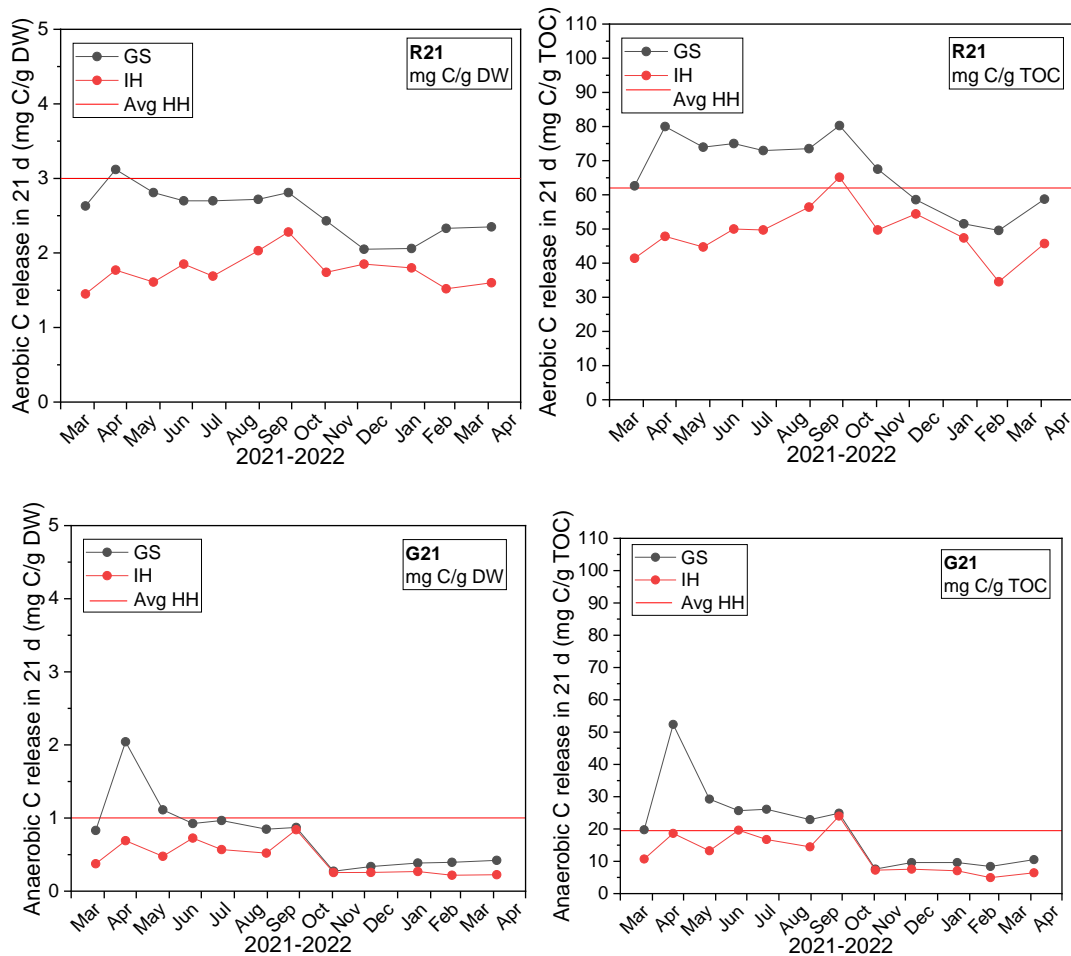
Figure 19. Cumulative release of organic carbon in 21 days under aerobic (top) and anaerobic (bottom) conditions. Left: C release normalized to unit dry weight, Right: C release normalized to unit total organic carbon (degradability). All data valid for 20 °C. Red line: Average value for fluid mud in the Port of Hamburg.

Organic matter decay under aerobic conditions (Figure 19, top panels), with oxygen available as terminal electron acceptor, is significantly higher than under anaerobic conditions (Figure 19, bottom panels), when fluid mud was incubated in the absence of oxygen. The factor between aerobic and anaerobic matter decay ranged between 1.3 and 7.7, with an average of 3.9. This difference reflects the lower energy gain and possibly the lower degradability of organic matter under anaerobic conditions. Given the low redox potential measured at both sites (Figure 13), it can be assumed that in situ organic matter decay is anaerobic. The higher aerobic organic matter decay rates illustrate the potential for C release if fluid mud is brought in contact with oxygen-rich water, e.g. during dredging interventions, possibly inducing oxygen minimum zones in the water. Aerobic and anaerobic organic matter decay (per unit dry weight, Figure 19, left) as well as anaerobic degradability (C release per unit organic carbon, Figure 19, top right) were in the lower range of values measured for fluid mud in the Port of Hamburg, while aerobic degradability (Figure 19, bottom right) was quite similar to average values measured in the Port of Hamburg. The temperature response of aerobic and anaerobic matter decay is well investigated and can be used to predict in situ carbon release in relation to in situ variation of temperature.

4.1.3.2 Abundance and composition of the microbial community

Total cell counts varied between 1.4×10^9 and 3.4×10^9 cells per ml fluid mud for site IH and between 8×10^8 and 4.4×10^9 cells per ml fluid mud at site GS (Figure 20). The higher variability at site GS was probably due to increased system dynamics at this site in relation to regular opening of the lock and import of fresh organic matter. A distinct seasonality could not be identified. At both sites, lowest cell counts were registered in September and November 2021 and highest cell counts were observed in December 2021 and January 2022. Compared to other aquatic habitats, cell counts are in the upper range.
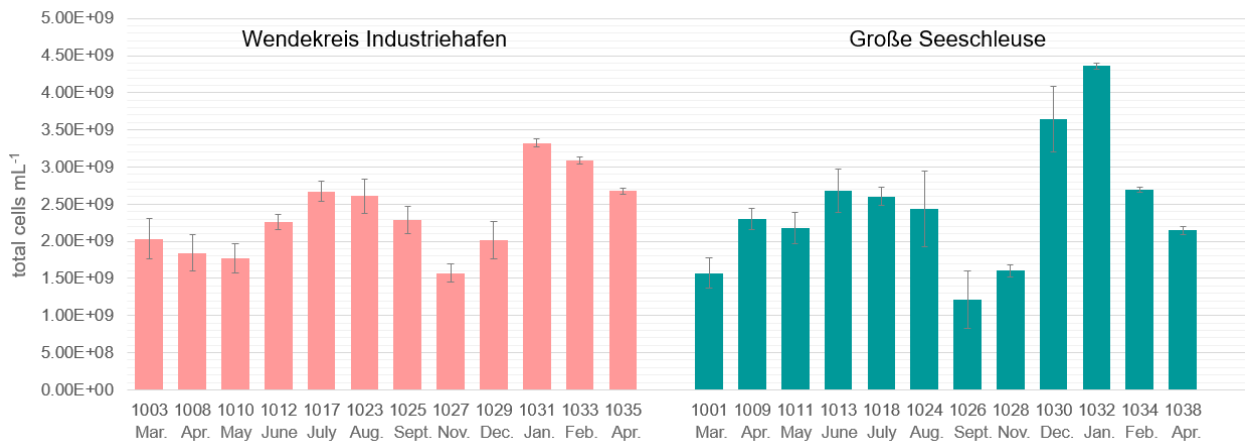
Figure 20. Total cell counts at sites IH (left) and GS (right) in the period March 2021 - April 2022.

Table 5. Cell counts in marine sediments.

Location	Total cell counts
The Port of Emden	$1.1 - 2.6 \times 10^9$
Coastal marine sandy sediments (Luna et al., 2022)	1.5×10^8
Coastal marine muddy sediments (Luna et al., 2022)	5.3×10^9
Organic-rich marine sediments (0-1 mbsf) (Schippers et al., 2012)	$10^9 - 10^{10}$

To illustrate the relationship between bacteria, archaea (amongst other processes responsible for methane production) and microalgae, derived from the quantitative PCR analysis (qPCR), all abundances per each sample were normalised to the group of bacteria (Figure 21). It is seen that in the fluid mud samples from the Port of Emden, bacteria represent the majority of the community, followed by the group of archaea, while at both sites microalgae account for the smallest part of the community (Figure 21). The distribution is clearly different from Hamburg sediments, in which the share of microalgae is by far higher, archaea are the least abundant group, and where strong spatial differences were found (Gebert et al., in prep.).

The **bacterial community** at both sites was highly diverse and differ significantly from each other. In both cases, over 60% are represented by genera with an abundance of less than 1.8% of the total hybridization product, as seen from the turquoise column (Figure 22). If these genera are disregarded, a clearer picture of the community's composition is obtained (Figure 23). While samples from March and April 2021 are still quite similar for the respective sites, the bacterial

community composition shifts significantly from May 2021 onwards. Samples from January, February and April 2022 show more similarity again for the respective site. The September sediment samples (1025 and 1026) show the lowest diversity at both sites. As seen from the diverging patterns, sites IH and GS feature different bacterial communities. A high number of various classical sulphate-reducing *Desulfobacterota* and others involved in biological sulphur cycle like *Sulfurimonas* and *Sulfurovum* were detected, plausible in a sulphur-rich environment under marine influence (Figure 15, bottom right).

The **archaeal community** of the field samples was also relatively diverse, although less than the bacterial community (Figure 24). Further, the archaeal communities at both sites resemble each other much more. Nanoarchael *Woesearchaeales*, Thermoplasmatotael *Marine Benthic Group D and DHVEG-1*, and Crenarchael *Nitrosopumilales* and *Bathyarchaeia* form the genera with the greatest abundances. Low abundant Archaea usually comprised less than 5% of the total archaeal community. Methane-producing *Methanosarciniales* appear more abundant at site IH which however did not reflect in higher anaerobic carbon (CH_4 and CO_2) release (Figure 19, bottom panel).

The total absence of any other genera than from the order of *Nitrosopumilales* in sample 1028 could be an artefact. However, also the pattern of the corresponding November sample from site IH (1027) is different from the rest of IH samples, suggesting a shared cause.

The **algal communities** at both sites was quite similar (Figure 25). In both cases species of the family of *Mediophyceae* (diatom algae) are the most abundant representatives, followed by genera of low abundance (< 2%) and members of the family of *Bacillariophyceae (*diatoms, too). However, clear differences were also detected: At site IH, the abundance of *Mediophyceae* was increased, also representatives of *Ploimida* were detected, whereas at site GS, the abundance of low abundance genera, *Bacillariophyceae* and other unspecified *Eukaryota* was increased. Also, *Centrohelida* were detected mostly at this site. With respect to the algal community composition, the November samples 1027 and 1028 stand out with presence of *Coscinodiscophytina*, another subdivision of diatom algae.

Relative abundance of bacteria, archaea and algae was quite dynamic over time (Figure 26, all normalised to sample 1001 from site GS). Bacterial abundance appeared to decrease over time at site GS, but not at site IH. Here, the samples collected in September and October stand out with very low abundance in all three groups. The relative abundance of all three groups was higher at GS than at IH at almost all times during the period of investigation. This could be related to increased input of fresh organic material in relation to opening of the great sea lock.

Principal coordinates analysis (PCoA) revealed that both field sites GS and IH and also the laboratory experiment (details in section 4.2.3.2) are characterised by microbial communities of distinct composition (Figure 27). Sample 1001 from site GS was closer to all samples from the laboratory study than to samples from site IH, which is plausible as this was the sample used as original field material for the laboratory study. The archaeal communities from the two field sites and the laboratory experiment are more similar to each other than the bacterial communities.
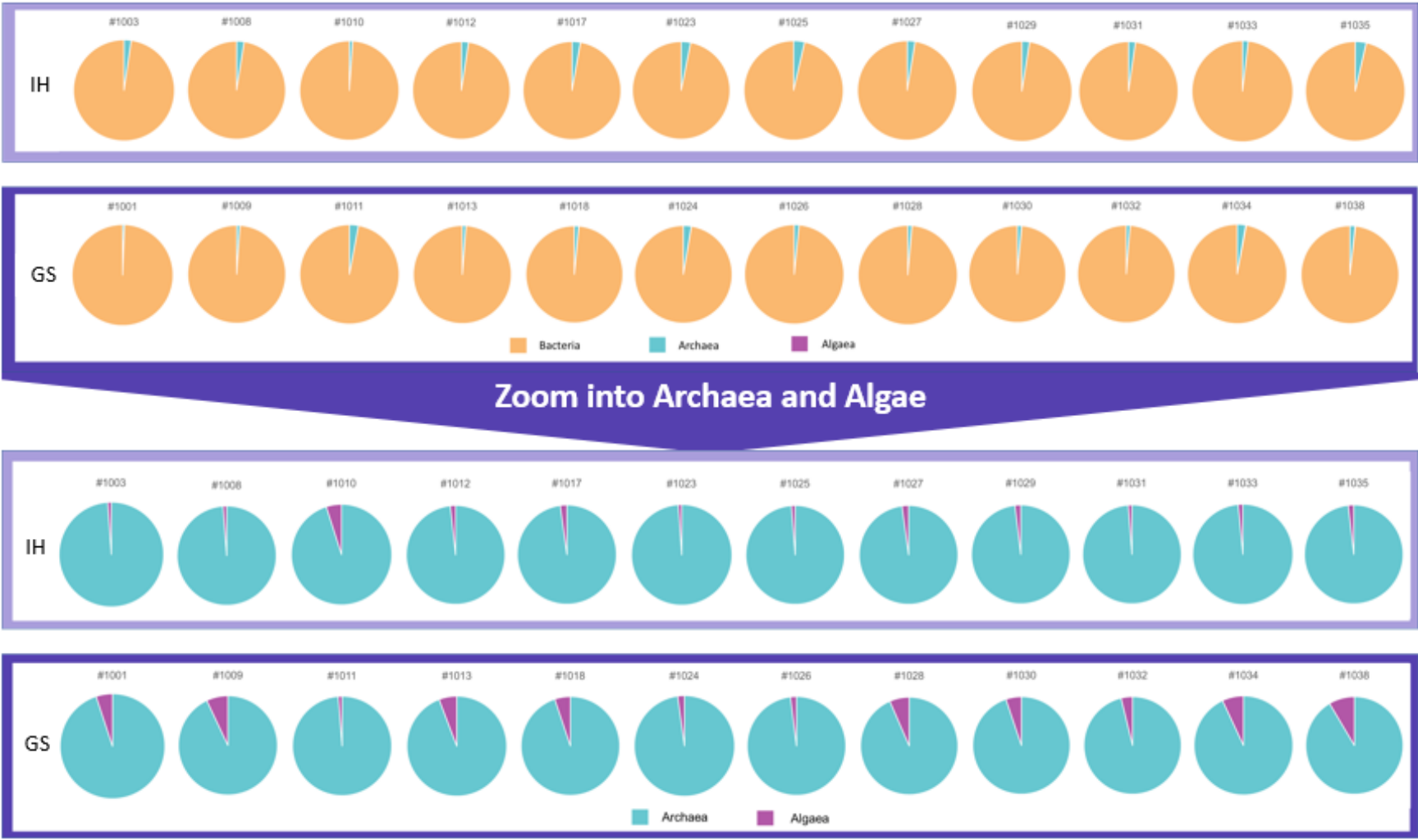
Figure 21. Relative abundance of bacteria, archaea and algae of the archaeal community at sites GS and IH.
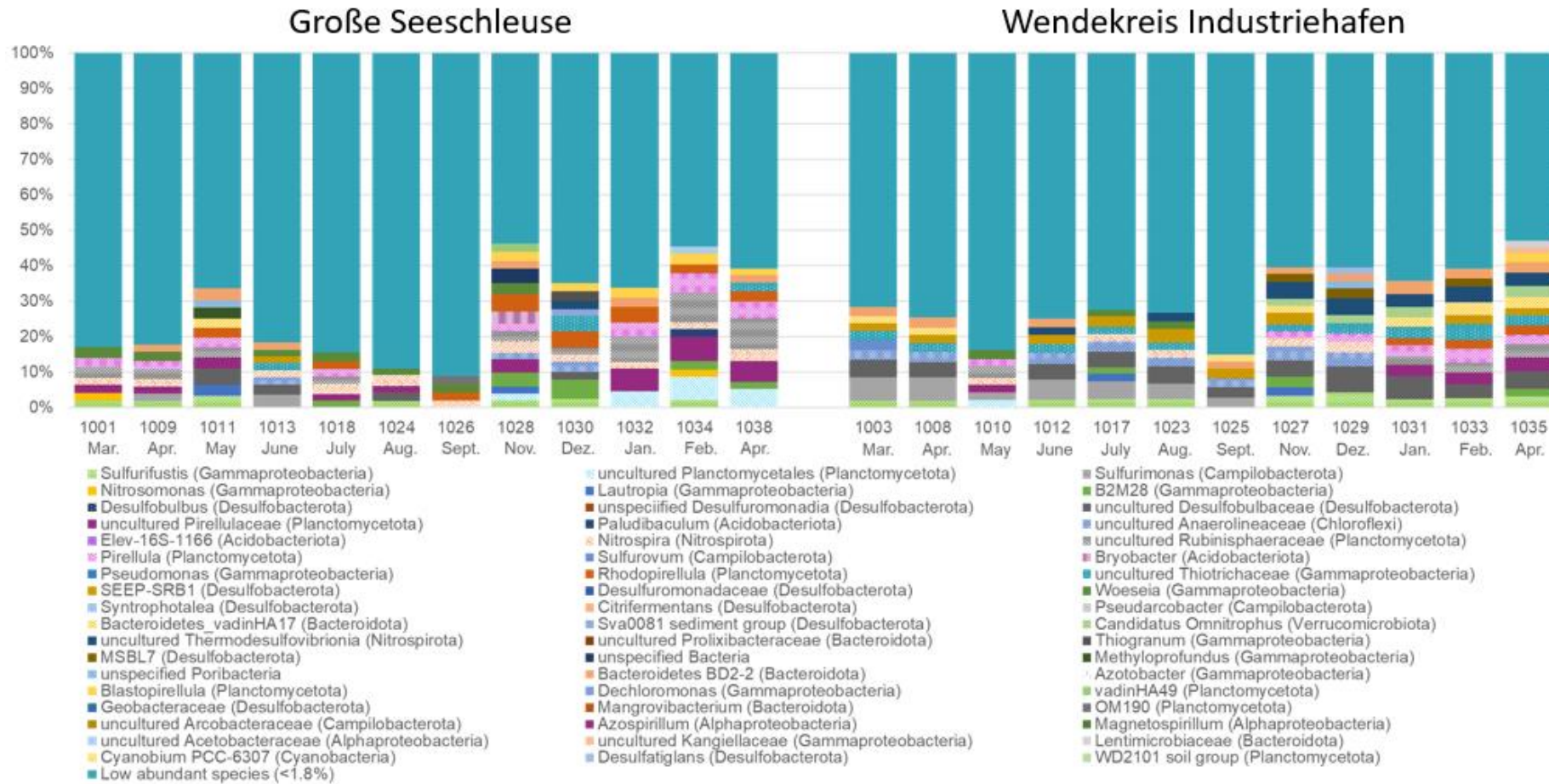
Figure 22. Composition of the bacterial community at site GS (left) and IH (right), including low abundances (< 1.8% of the hybridization product).
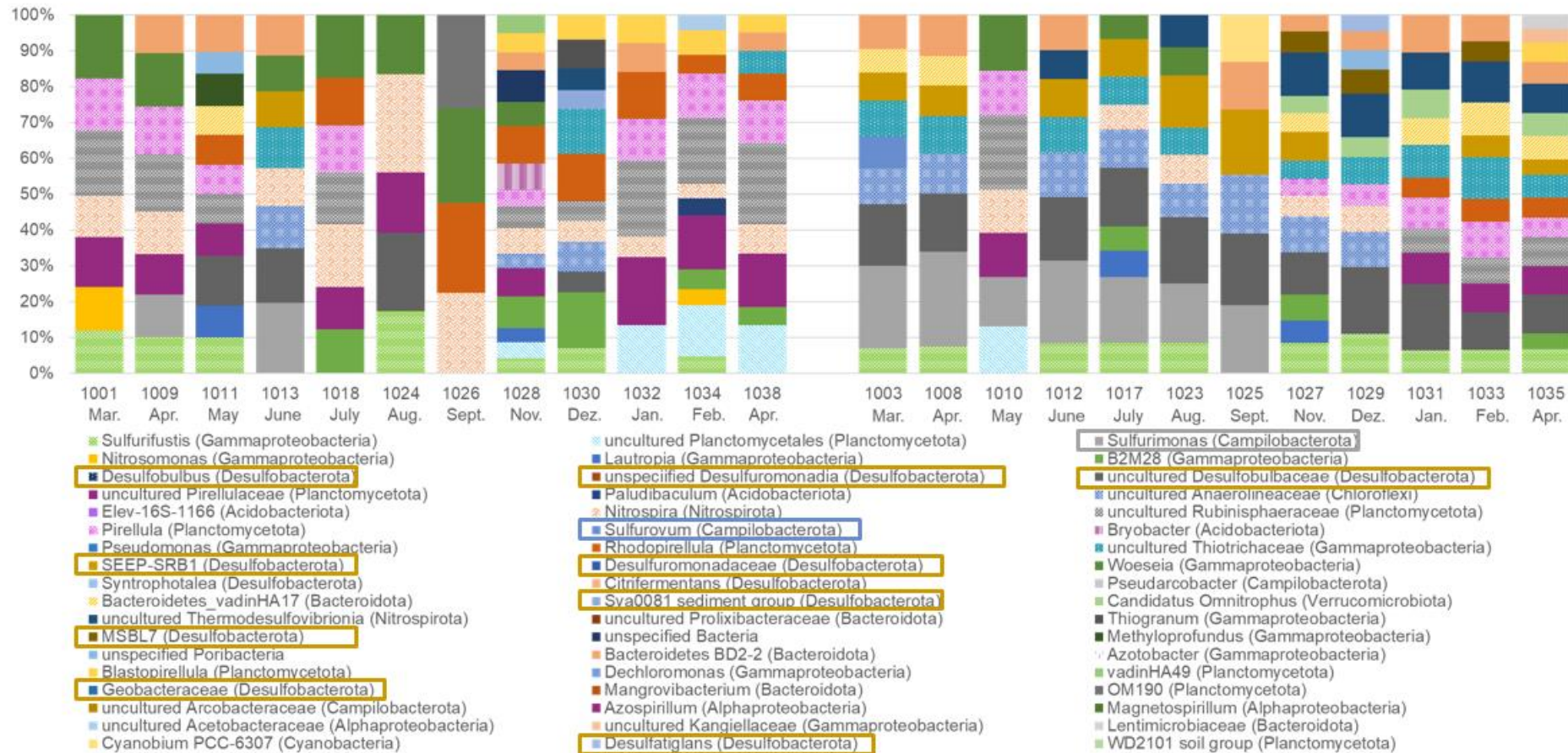
Figure 23. Composition of the bacterial community at site GS (left) and IH (right), excluding low abundances. Brown boxes: genera belonging to the *Desulfobacterota*, blue box: *Sufurovum*, grey box: *Sulfurimonas*.
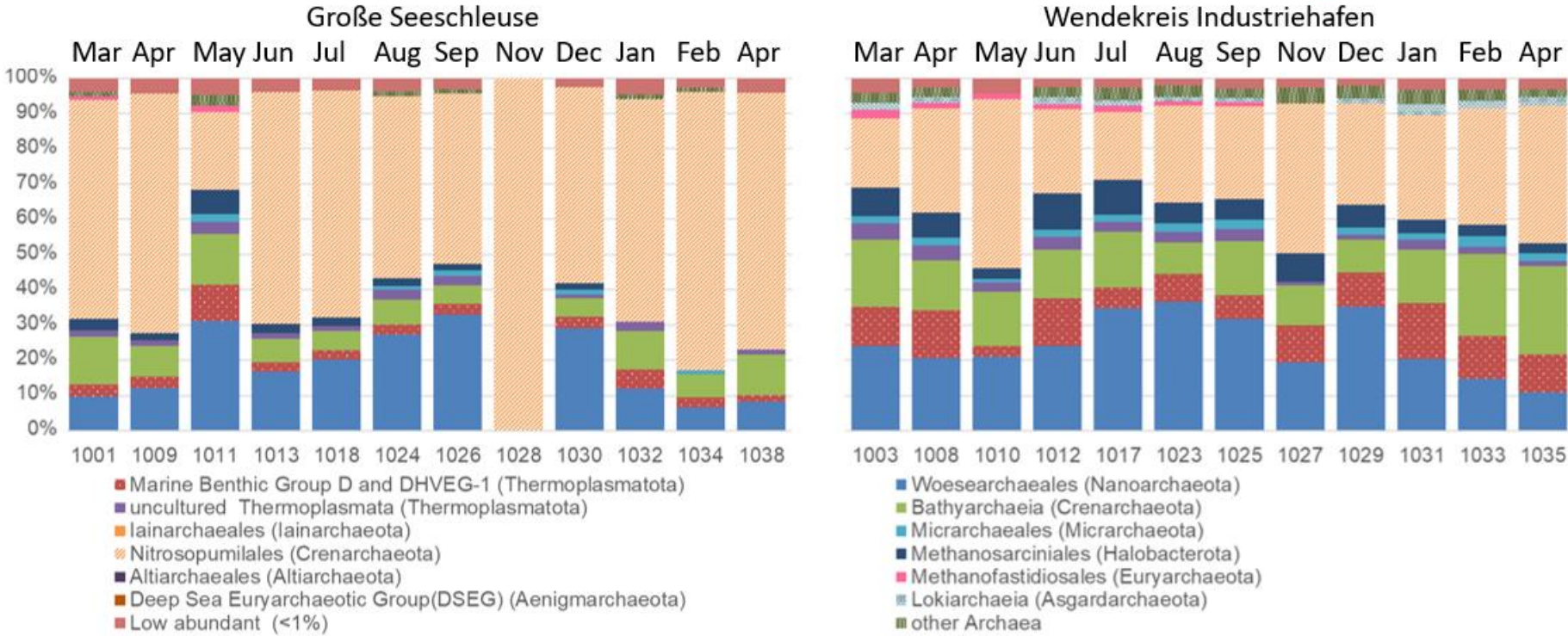
Figure 24. Composition of the archaeal community at site GS (left) and IH (right).
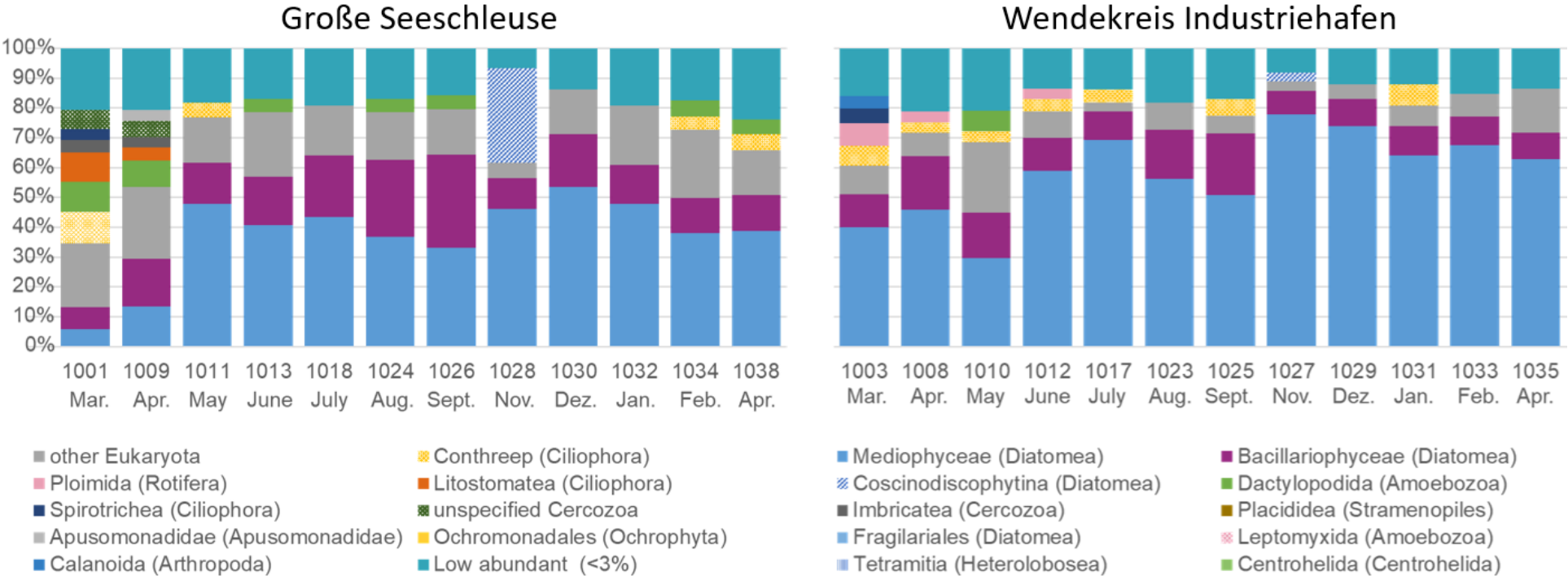
Figure 25. Composition of the algal community at site GS (left) and IH (right).

Figure 26. Relative abundance of bacteria, archaea and algae at sites GS (top) and IH (bottom). All data normalised to field sample 1001.
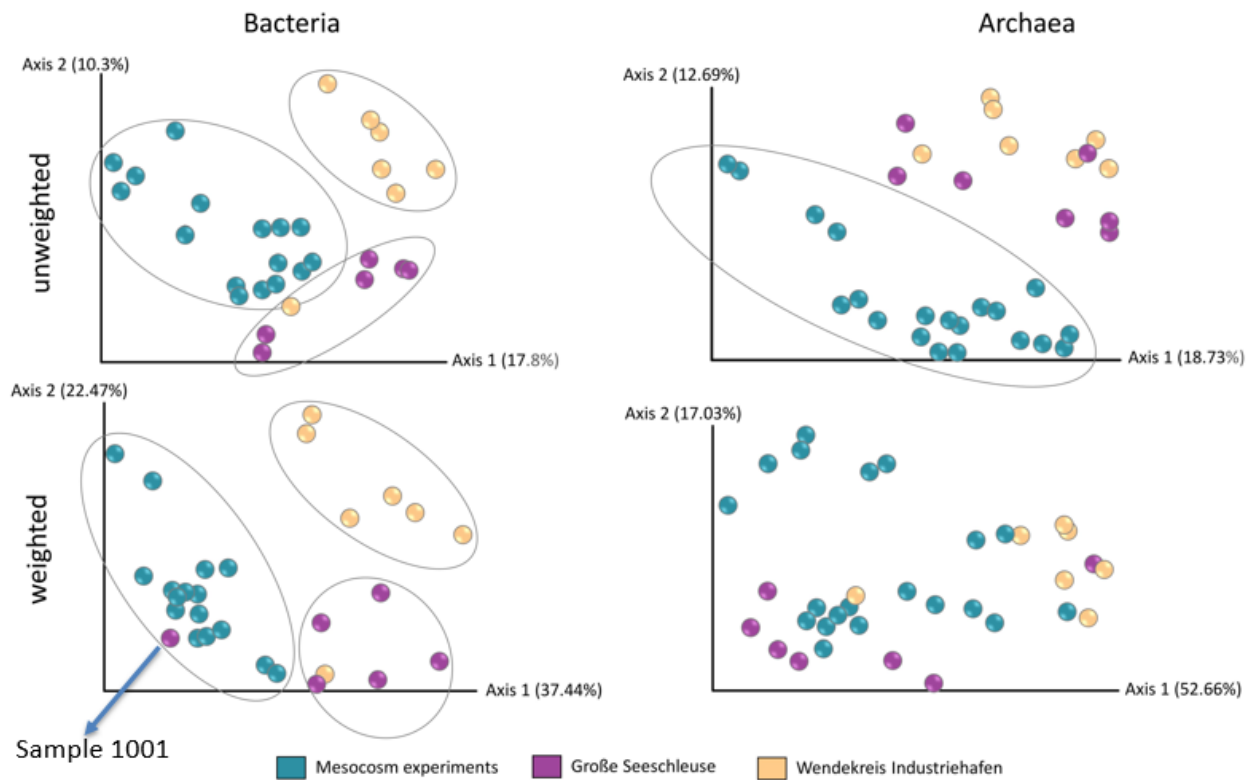
Figure 27. Intersample similarity analysis (Principal Coordinates Analysis (PCoA) plots). Weighted PCoA (top panel) includes abundance of genera, unweighted PCoA (lower panel) considers only presence or absence of genera.

4.1.3.3 Concentration and composition of extracellular polymeric substances (EPS)

EPS were analysed with respect to their main components, i.e. DNA, proteins, neutral and acidic polysaccharides, and lipids. As the lipid fraction dominated total concentrations, EPS composition is depicted including and excluding lipids.

Lipids represent the dominant component of EPS at sites GS and IH and in fluid mud in the Port of Hamburg (Figure 28). The second largest contributor are the acidic polysaccharides. Overall, EPS composition appears to differ in the samples from the Port of Hamburg. For example, a higher average share of lipids in relation to acidic polysaccharides and a higher share of uronic acids in relation to all other components was observed, but a lower share of protein in relation to DNA, and a lower share of DNA, proteins and neutral polysaccharides in relation to acidic polysaccharides(Figure 29).
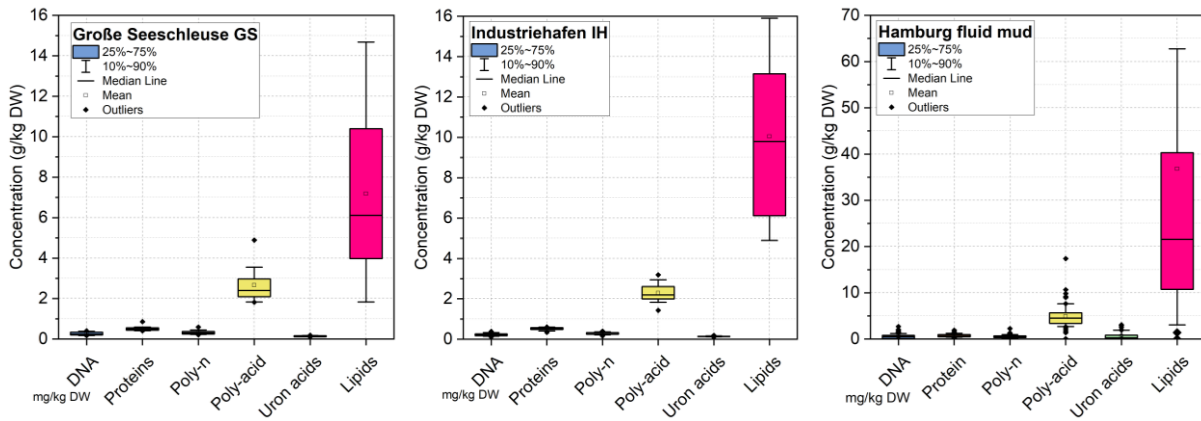
Figure 28. Composition of EPS including lipids for in-situ samples from sites GS (left, n = 12), IH (middle, n = 12) and the Port of Hamburg (right, n = 61). Note that DNA concentrations are given in mg/kg DW. For data from the Port of Hamburg, concentrations of lipids > 70 g/kg DW are not shown.
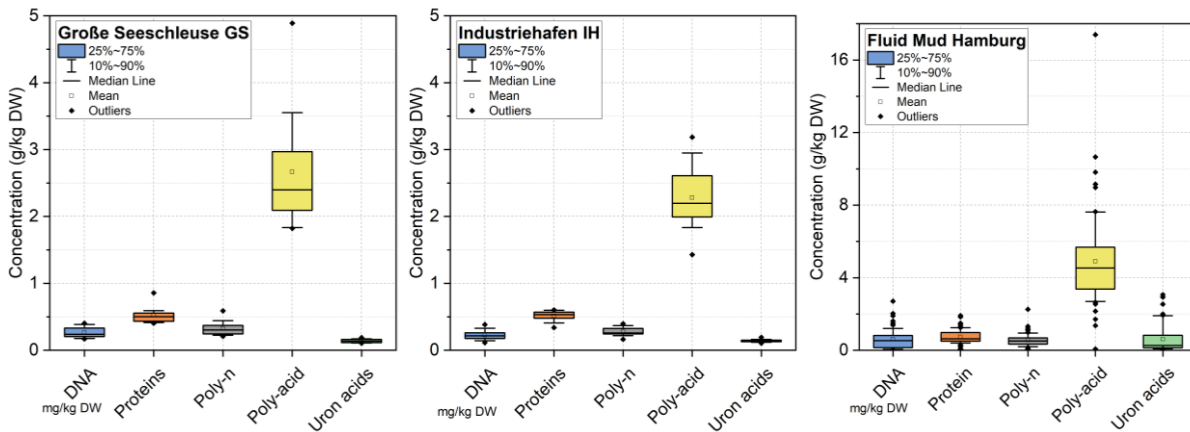
Figure 29. Composition of EPS excluding lipids for field samples from sites GS (left, n = 12), IH (middle, n = 12) and the Port of Hamburg (right, n = 61).

Total EPS content was slightly higher at site GS than at IH, but at both sites significantly lower than found in the Port of Hamburg. Here, very high concentrations of lipids were observed, leading to very high total EPS contents that on average were 3.5 times higher than found in the Port of Emden (Figure 30). Excluding lipids reduced this ratio to around 2.
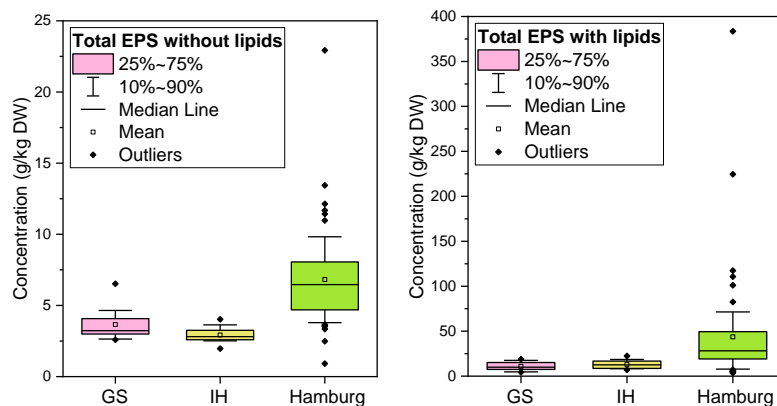
Figure 30. Concentration of total EPS excluding (left) and including (right) lipids for in-situ samples from sites GS (left, n = 12), IH (middle, n = 12) and the Port of Hamburg (right, n = 61).

The concentration of EPS showed a seasonal variation, starting with lower values in spring 2021, elevated values until December 2021 and a drop again in the later winter months (Figure 31). This seasonality likely reflects growth and die-off of the microbial community as a result of seasonal growth and die-off of phytoplankton.
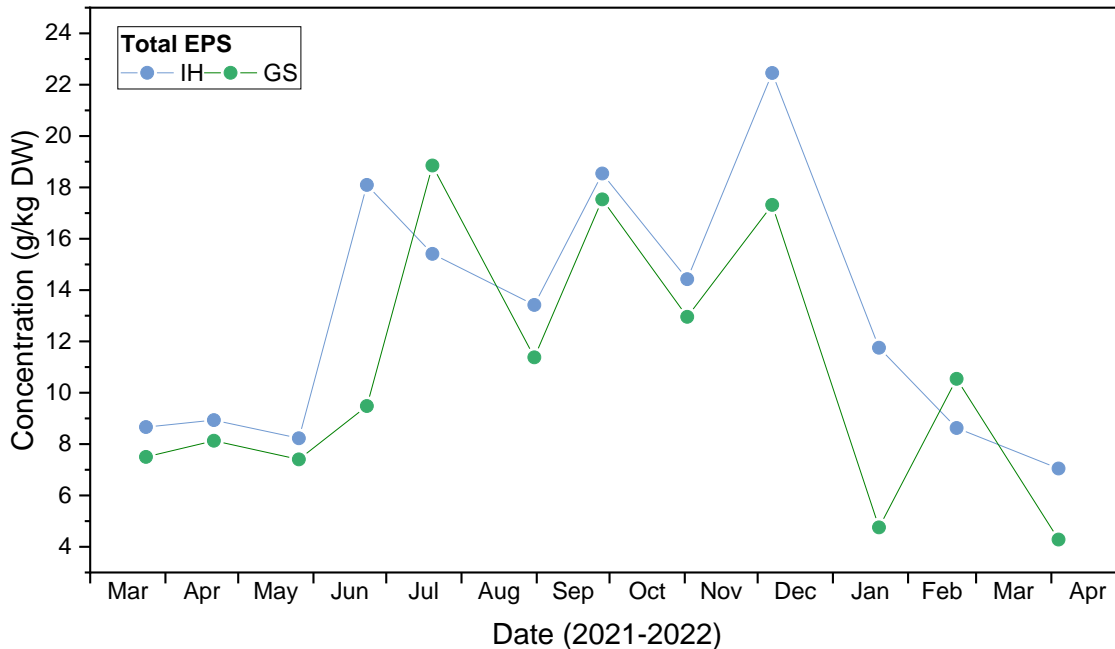
Figure 31. Concentration of total EPS over time in in-situ samples from sites GS and IH.

4.2 Laboratory study

Sample 1001 from site GS was selected for the long-term laboratory incubation, investigating the effect of increased shares of freshwater on fluid mud properties under conditions of weekly maintenance. Maintenance dredging (recirculation) was mimicked by agitating the fluid mud using a vane once weekly for two hours (see section 2.2). From March to November 2021, basic properties such as pH, EC, density and yield stresses, but also the microbial community composition and organic matter degradation were investigated at six points in time (t0 to t5).

4.2.1 Physical properties of fluid mud

4.2.1.1 Density and dry mass

As intended, the **density** of the fluid mud in the five mesocosms was adjusted to the same value that also remained more or less constant over time (Figure 32). The decrease over time can be attributed to evaporative loss during vane mixing.

The **dry mass** ranged between 11.5 and 12% of the wet weight and showed a very small increase over time, likely due to evaporation during the weekly mixing events. Differences between the samples are likely due to uncertainty in the analysis in relation to the very high water contents and possible incomplete homogenization of the mesocosm sample. For all practical matters, the differences between samples and over time can be considered negligible, especially when compared to the variability in the field (Figure 9).
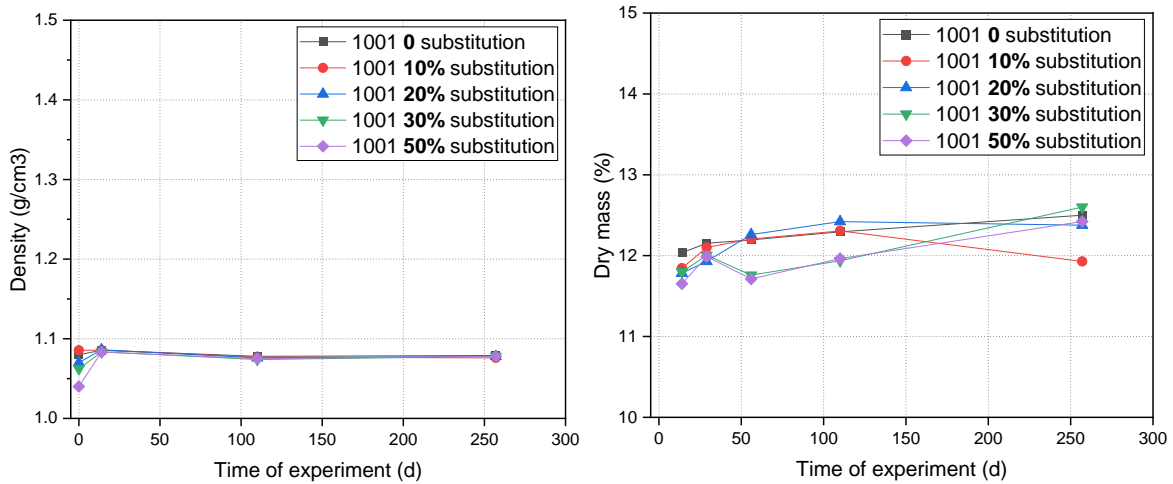
Figure 32. Density and dry mass measured over time over time of experiment.

4.2.1.2 Yield stress

Both fluidic (FYS) and static (SYS) yield stress did not show significant changes in any of the mesocosms over the time of incubation (Figure 33) but remained very close to the values of the original field sample 1001 from March 2021 (Figure 10). Exchange of saline for freshwater had no significant impact on the yield stresses.
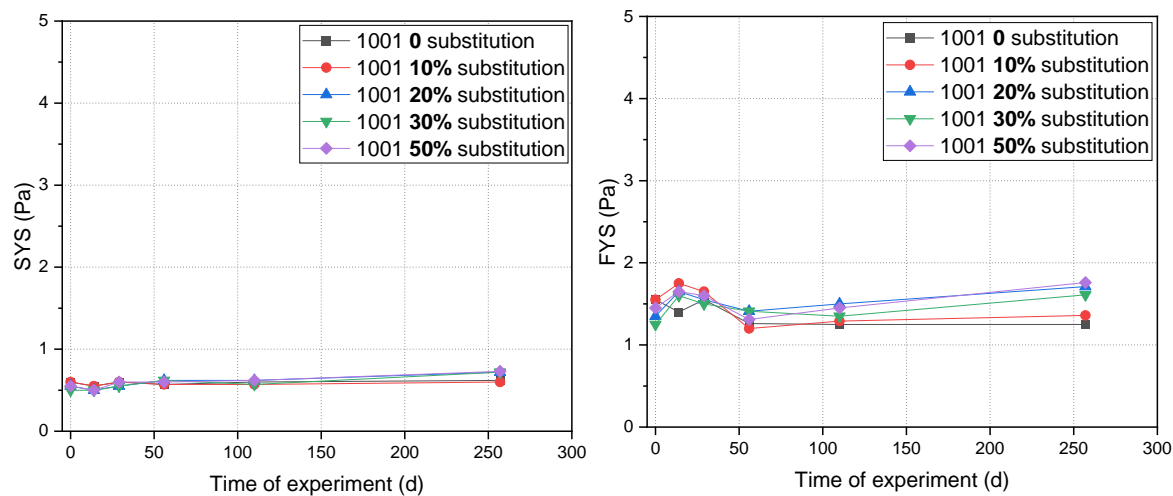
Figure 33. Static (left) and fluidic (right) yield stress over time of experiment.

4.2.1.3 Settling rate

Throughout the time of incubation, significant changes in settling rates were observed for all levels of substitution of original water with fresh water. In general, settling rates first decreased between time points t0 and t3, and then increased again, indicating changes in particle properties over time (Figure 34).

0% substitution: an initial decreasing trend is observed until the curve flattens at t5.

10% substitution: from t0 until t5 the settling velocities show a decreasing trend whereas at t5 there is a considerable increase until approximately 21 mm/d.

20% substitution: from t0 to t3 a decrease can be observed followed by an increase to similar values for t4 and t5 (12 mm/d).

30% substitution: from t0 to t2 a similar decrease characterized this series. However, the starting settling velocity at t0 is the lowest measured in the series. At t3 this samples shows the highest settling velocity. At t4 a slight decrease followed by a new increase at t5 is observed.

40% substitution: similarly to the previous series an initial decrement from t0 to t3 emerges. While the value at t4 is similar to t3, the t5 value is higher with 17 mm/d.

Chemical properties such as pH and redox potential showed significant changes over time (section 4.2.2), indicating changes in the biogeochemical boundary conditions within the mesocosm. It is likely that this impacts the particle-particle interactions through changes in redox-sensitive elemental speciation and therefore the settling rates.
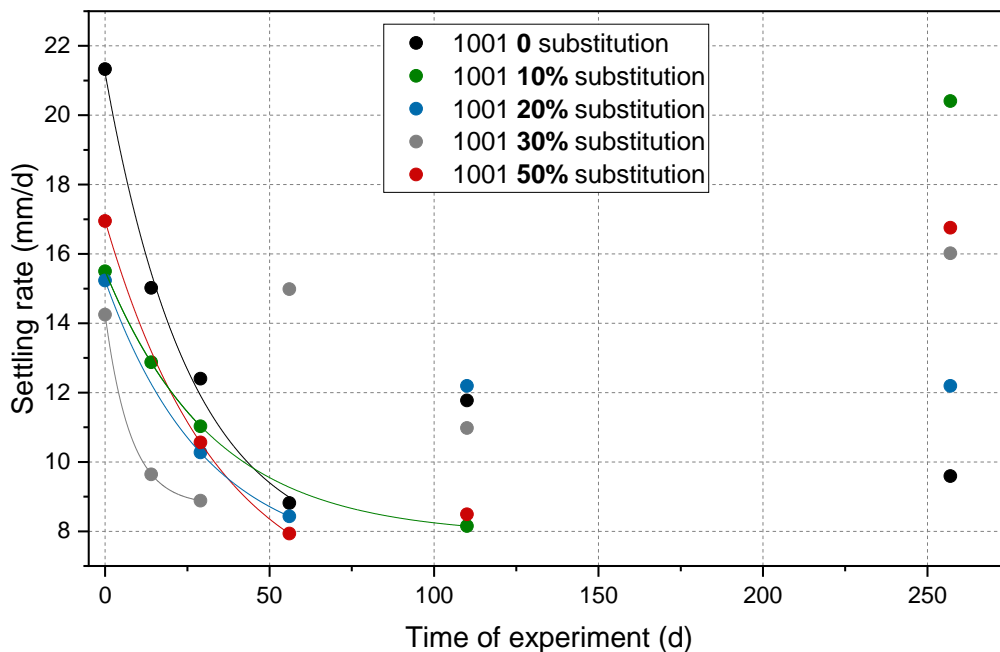
Figure 34. Settling rates for the different levels of substitution with freshwater and over time of experiment.

4.2.2 Chemical properties of fluid mud

4.2.2.1 pH value and electrical conductivity (EC)

pH values for all subsamples ranged from 7 to 7.8. The sample that was substituted with 10% fresh water showed the highest value at time point t4 (July 2021). Overall, pH values did not vary significantly until t4, i.e. until four months after the beginning of the incubation. Only by the time of t5 in November 2021, a significant decrease was observed, likely indicating hydrolysis and inhibited methanogenesis during the later stages of the experiment (Figure 35, left panel).

EC values, representing the sample's salinity, was rather constant for all subsamples over time, indicating that the effect of exchange of original saline water with freshwater provided a stable boundary condition for the duration of the experiment. The step of 50% substitution indeed almost halved the EC value as compared to the original undiluted sample 1001 (Figure 35, left panel).
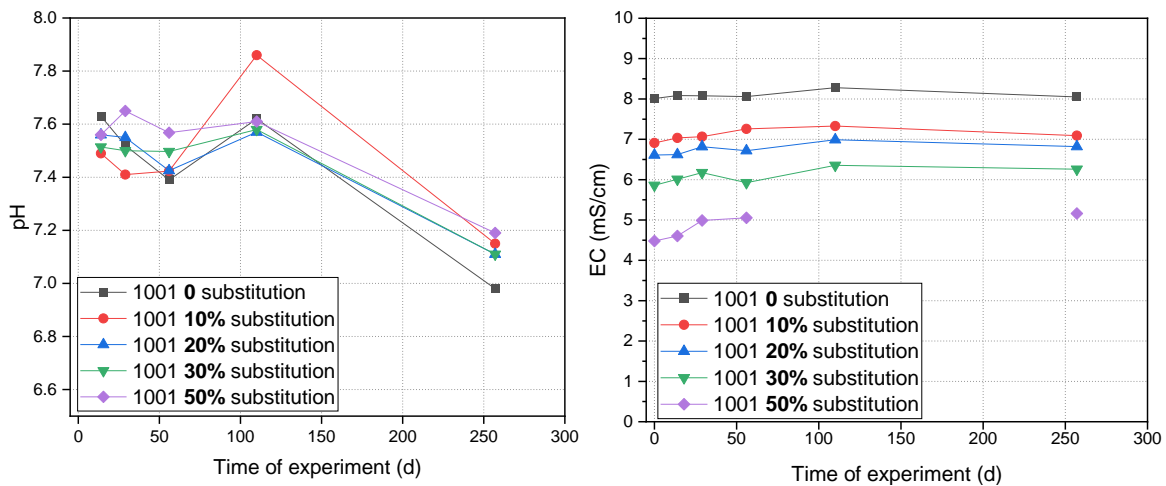
Figure 35. pH and EC over time of experiment.

4.2.2.2 Redox potential

Under field conditions, fluid mud almost always maintained negative redox potentials (Figure 13). The same was observed for the mud in the mesocosms (Figure 36, left panel), which, however, displayed significant dynamics with redox potentials first decreasing and then increasing towards the last sampling moment t5 (Nov 2021). This possibly indicates that the oxygen-consuming processes occurred at increasingly lower rates. This observation was supported by the decrease in organic matter degradation over time of experiment (Figure 37).

The reducing potential of the fluid mud is high. This was demonstrated by a separate measurement when the redox potential was analysed before and after two hours of mixing with the vane (Figure 36, right panel). It is seen that two hours of complete mixing of the mesocosm content under the open atmosphere increased the redox potential only slightly. This also explains the negative values in the field even under conditions of recent dredging and hence exposure to atmospheric oxygen.
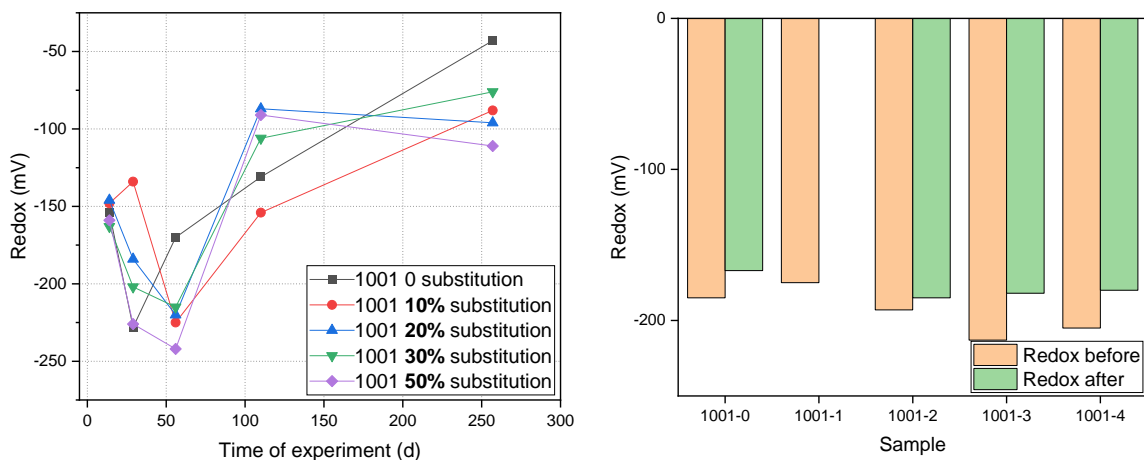
Figure 36. Redox potential over time of experiment (left) and effect of sample mixing (vane, 2 hours) on the redox potential (right).

37

4.2.3 Biological properties of fluid mud

4.2.3.1 Degradation of organic matter

At almost all substitution levels steps, as well as in the undiluted reference, an increase in organic carbon release towards day 69 of the experiment was observed, followed by a decrease to values below the one registered for the original sample 1001 (t0; Figure 37, left). This means that the transfer of the field sample to the conditions of the laboratory and mimicking the maintenance measures (weekly shearing) initially enhanced organic matter decay. There was no systematic difference between the different levels of freshwater substitution, i.e. exchange of salt water with fresh water (Figure 37, right panel). The only outlier was the substitution level of 10% which showed a very strong increase in organic matter decay between t1 and t2. It is assumed that unintentional spill of ethanol used for disinfecting sampling equipment led to a die-off of parts of the biomass in this sample, resulting in enhanced mineralization rates by the consumer population. Over time, carbon release declined to the level of the other samples.
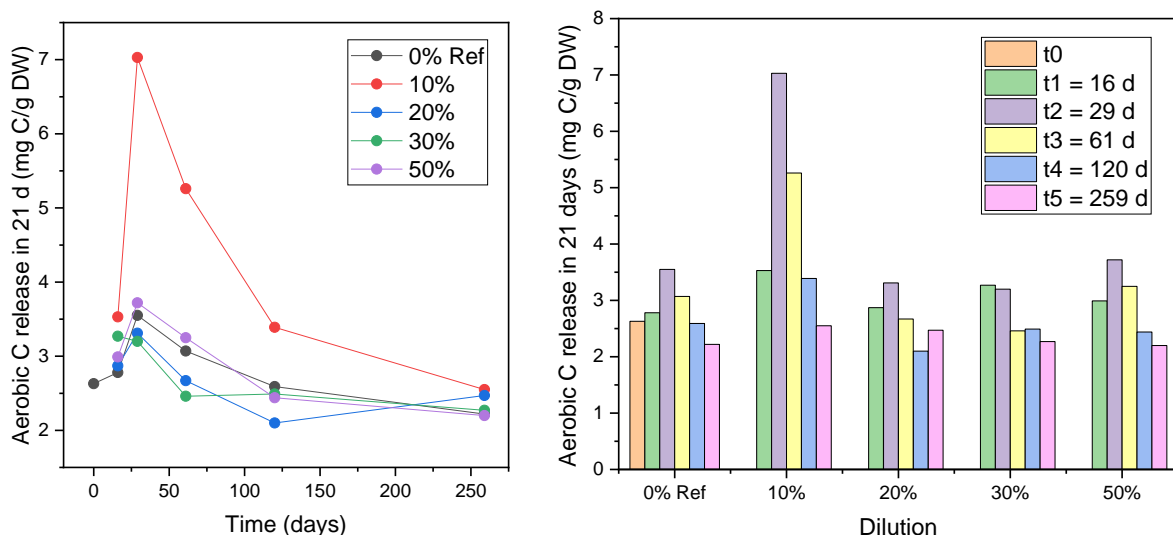
Figure 37. Cumulative release of organic carbon in 21 days over under aerobic conditions. Left: Data grouped over time of laboratory incubation. Right: data grouped with respect to degree of dilution.

4.2.3.2 Abundance and composition of the microbial community

In relation to the original sample 1001 (Figure 20), **total cell counts** were increased in all substitution levels until sampling point t3 (60 days after start of incubation) and decreased to slightly lower levels thereafter (Figure 38). Overall, a decreasing trend over time was observed. Differences between levels of substitution with freshwater were larger but not systematic until time point t3 and became small thereafter. The initial increase is attributed to laboratory conditions increasing microbial growth rates, for example higher temperatures. In the longer term, the system is characterized by a depletion of available organic matter, presumably causing a decrease in cell counts. This trend was also found for the aerobic degradation of organic matter shown in Figure 37.

As in the field samples, the community in the laboratory mesocosms was dominated by bacteria (Figure 39). This was true for all levels of freshwater substitution and over the entire duration of the experiment (8 months). Towards time point t3 (2 months) the share of archaea in relation to

algae seemed to increase, but then decreased thereafter. No systematic differences between the levels of substitution with freshwater were detected.

As in the field samples (Figure 23), the **bacterial community** in the laboratory incubations were very diverse and characterised by a very high share of low abundance genera (Figure 41). However, the experimental setting, changing the environmental conditions compared to the field setting, clearly shifted the community composition (see 0% substitution, far left). The substitution level of 10% exceptional presence of *Desulfolobus* species from sampling point t2 onwards, matching the exceptional increase in respiratory activity (Figure 37) which was assumed to be due to the accidental addition of ethanol to the mesocosm and the subsequent availability of easily degradable organic matter. The observations match the recent literature suggesting that bacteria in the phylum *Desulfobacterota* comprise heterotrophic species (Waite et al., 2020). The different substitution levels vary strongly in their community composition, however, some genera were also present in all levels over time and did not vary much with respect to abundance, such as *Nitrospira* or *Bryobacter* species.

Compared to the bacterial community, the **archaeal community** appears to be more stable and resilient to changes in freshwater admixture (Figure 42). This is in line with the field observations, where also the variability within Archaea was significantly less than within Bacteria (Figure 23 and Figure 24). While 10% and 20% substitution levels mostly resemble the reference sample, 30% and 50% are characterized by increased share of *Bathyarcheia* (green column), and these differences appear stable over time. Again, time point t3 in the 10% substitution level shows an exceptional composition with significant presence of *Methanosarciniales* (dark blue column), which normalized towards the end of the experiment. This coincides with an increase of redox potential and decrease of pH at the last sampling point (Figure 35 and Figure 36), clearly indicating changes in the geochemical boundary conditions. Overall, abundances of main genera apart from *Nitrosopumilales* appeared to increase throughout the experiment but then dropped at the last sampling point t5, while the abundance of *Nitrosopumilales* increased again.

The **algal community** in the mesocosm samples consisted mainly of *Mediophyceae*, *Bacillariophyceae*, *Conthreep*, other unspecified Eukaryota and genera with low abundance (< 0.8%; Figure 43). The abundance of the different algal orders changed in response to the incubation time. *Mediophyceae* and *Bacillariophyceae* appeared to first increase and then decrease again over time of incubation. The input of different amounts of freshwater did not have a systematic effect on the composition of the algal community. Sampling time point t3 stands out again at the 10% substitution level, showing a strong increase of *Conthreep*, likely associated with an accidental addition of ethanol as explained above.
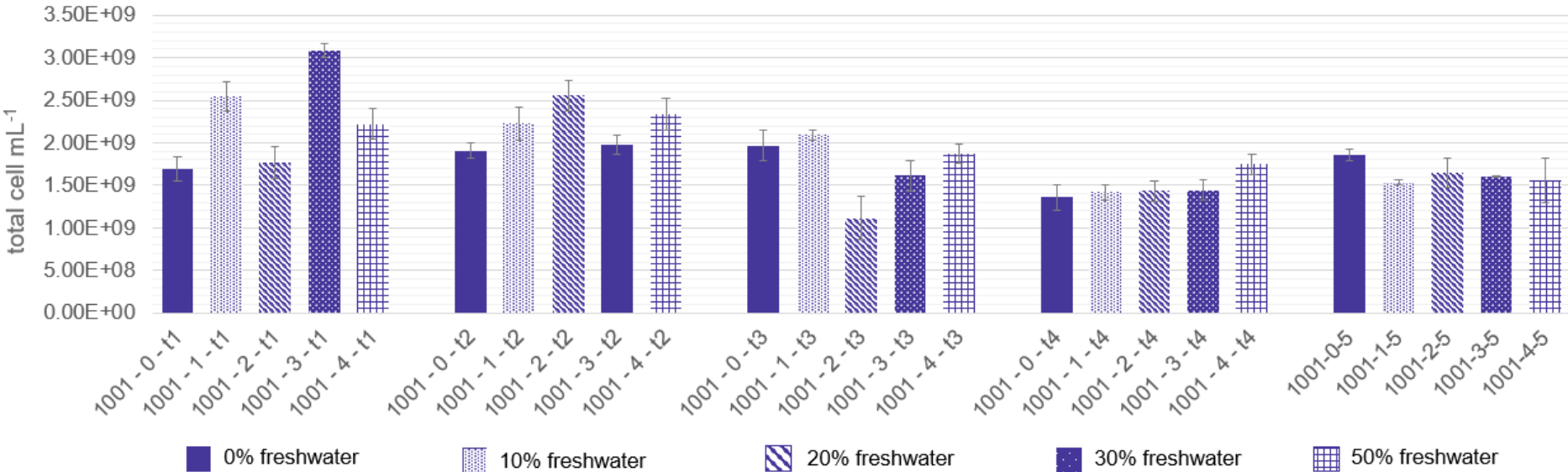
Figure 38. Total cell counts in relation to level of substitution with fresh water and over time. Error bars = standard deviation.
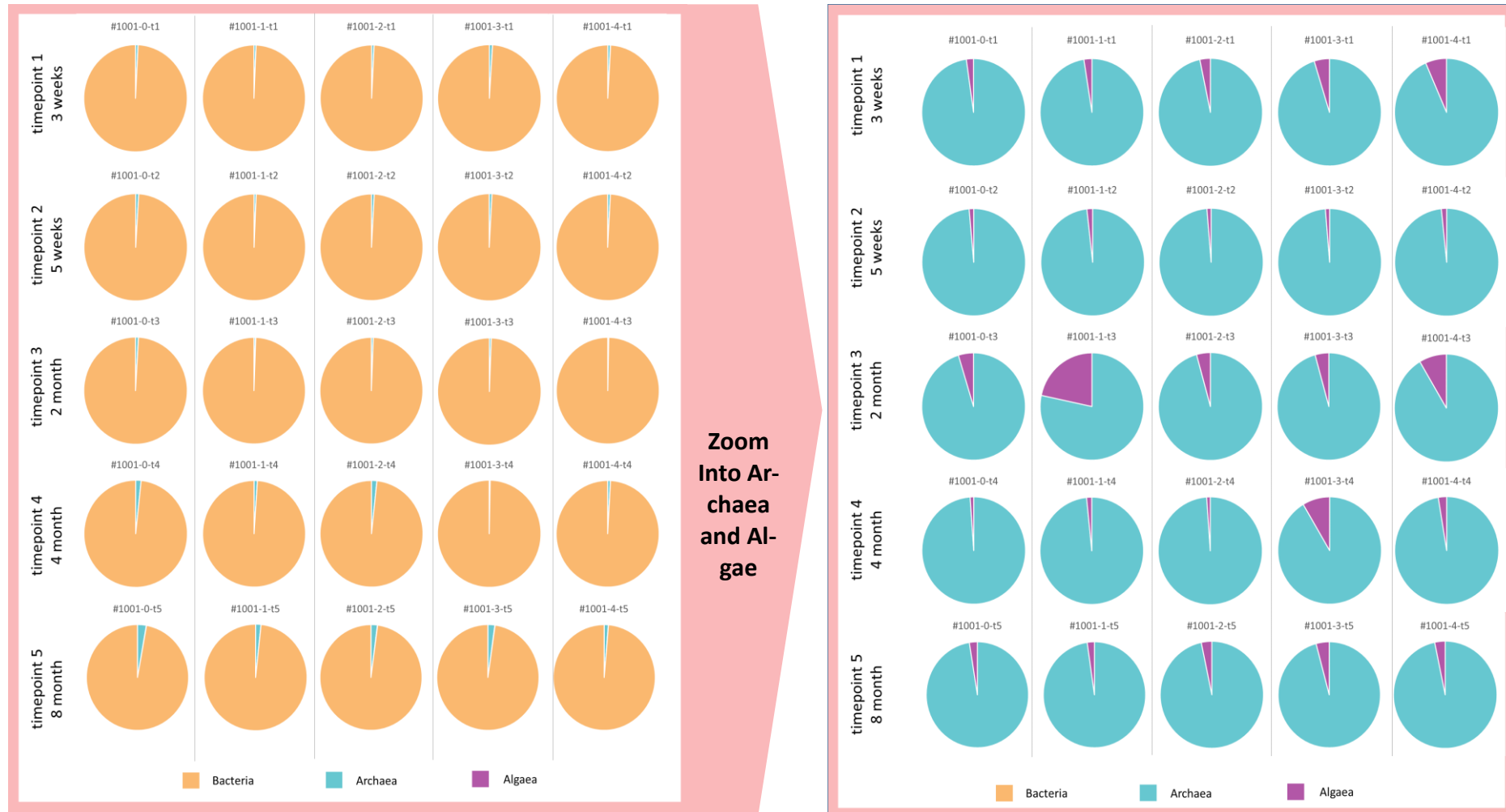
Figure 39. Relative abundance of bacteria, archaea and algae of the archaeal community for each freshwater substitution level (left to right) and over time of experiment (top to bottom).
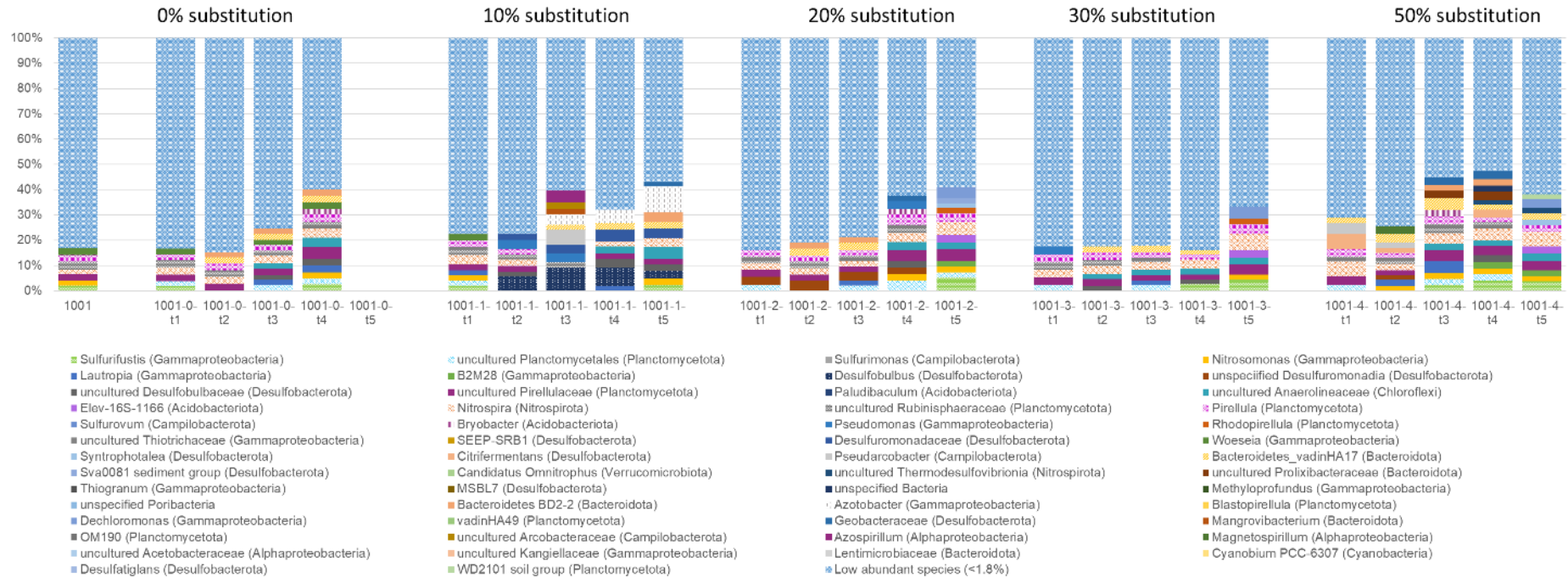
Figure 40. Composition of the bacterial community in relation to level of substitution with fresh water and over time, including low abundances (< 1.8% of the hybridization product). No data available for sample 1001-0-5.

Figure 41. Composition of the bacterial community in relation to level of substitution with fresh water and over time, excluding low abundances. No data available for sample 1001-0-5.
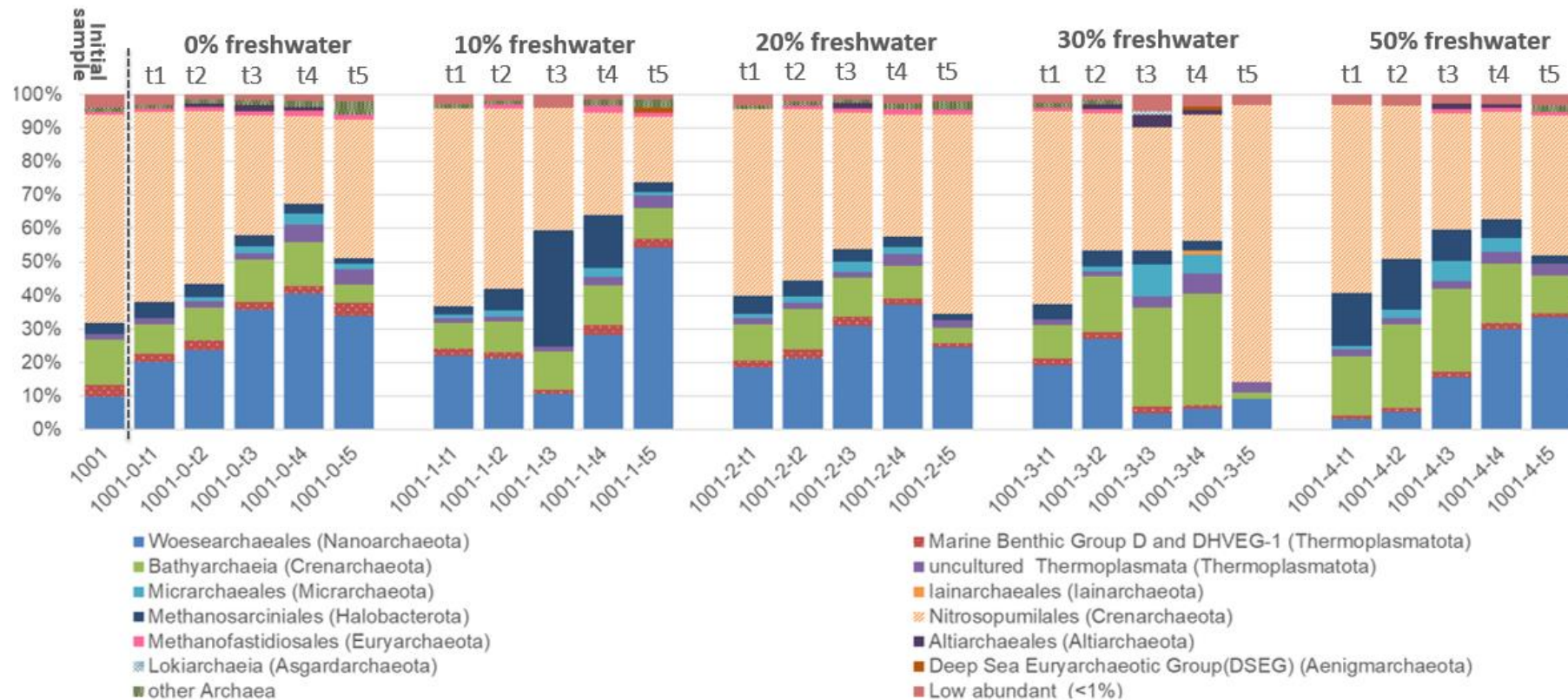
Figure 42. Composition of the archaeal community in relation to level of substitution with fresh water and over time. Top: including low abundances (< 1.8% of the hybridization product). Bottom: excluding low abundances.
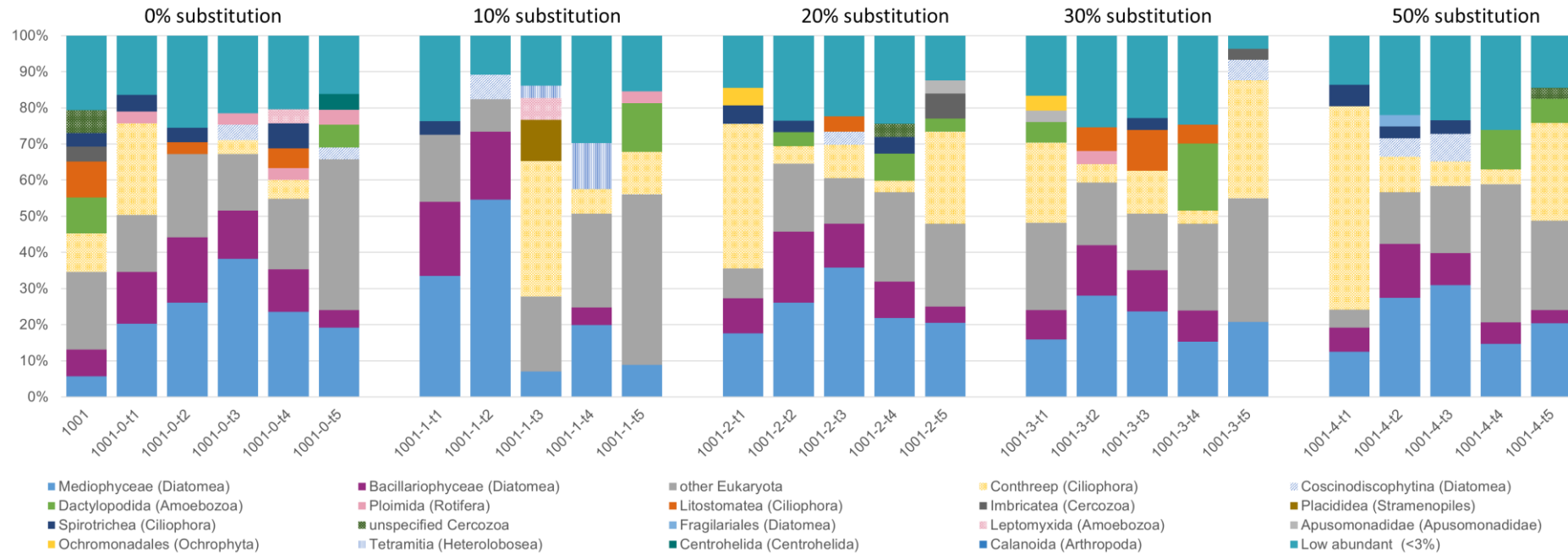
Figure 43. Composition of the algal community in relation to level of substitution with fresh water and over time.

.

Exchange of saline water for freshwater reduced relative quantities of bacteria and archaea with increasing level of substitution, but also in the unsubstituted sample (Figure 44). This effect was most clearly visible at time point t1, corresponding to three weeks after the onset of the experiment. Thereafter, no systematic effect of substitution level on relative abundance was observed. Towards the end of the incubation period, relative abundances of archaea and algae increased again. The patterns indicate an immediate impact but thereafter also an adaptive response to the rigorously changed environmental conditions (from the field to the laboratory situation). The long-term similarity after 8 months suggests a levelling effect of the ex-situ conditions for bacterial growth and activity, overruling the effect of the different levels of freshwater admixture.
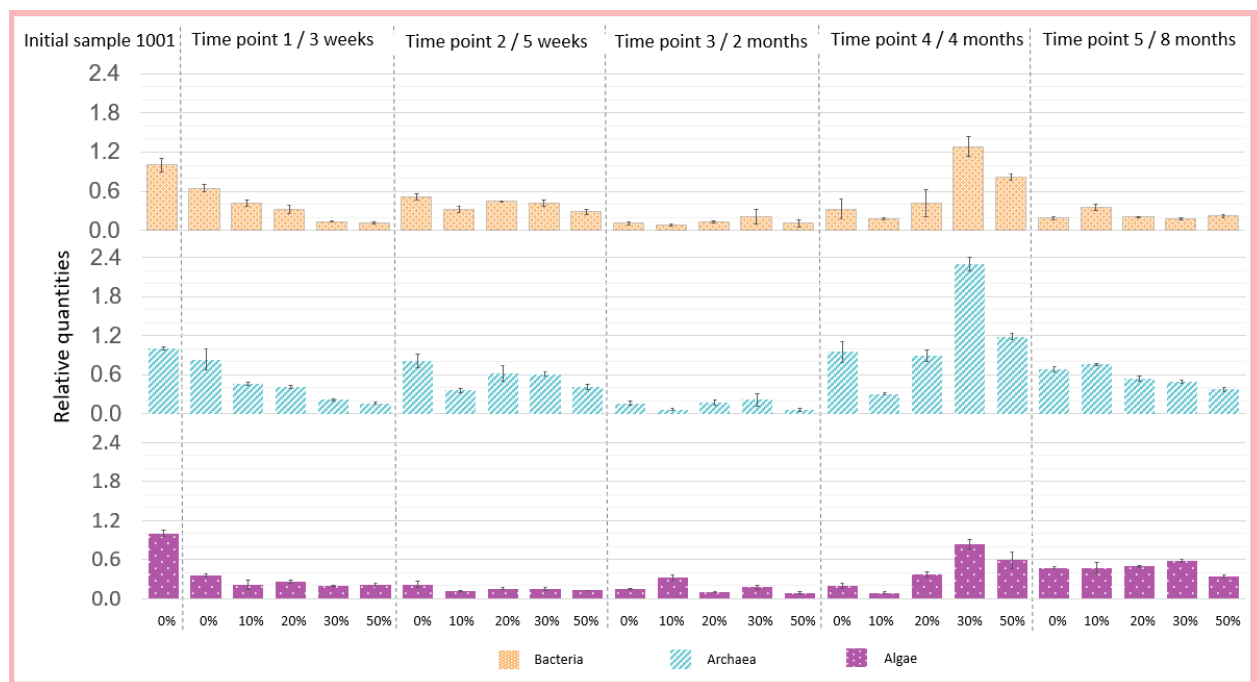
Figure 44. Relative abundance of bacteria, archaea and algae, for each freshwater substitution level and over time of experiment. All data normalised to original field sample 1001.

Principal coordinates analysis (PCoA) of the laboratory incubation samples showed that there was no grouping of the microbial community composition with level of substitution of saline water with freshwater, but rather that the mesocosm samples as a whole are distinct from the two sets of field samples. This supports the earlier assumption that the laboratory conditions are a strong driver of community composition and may overrule effects of variability in the fraction of freshwater.
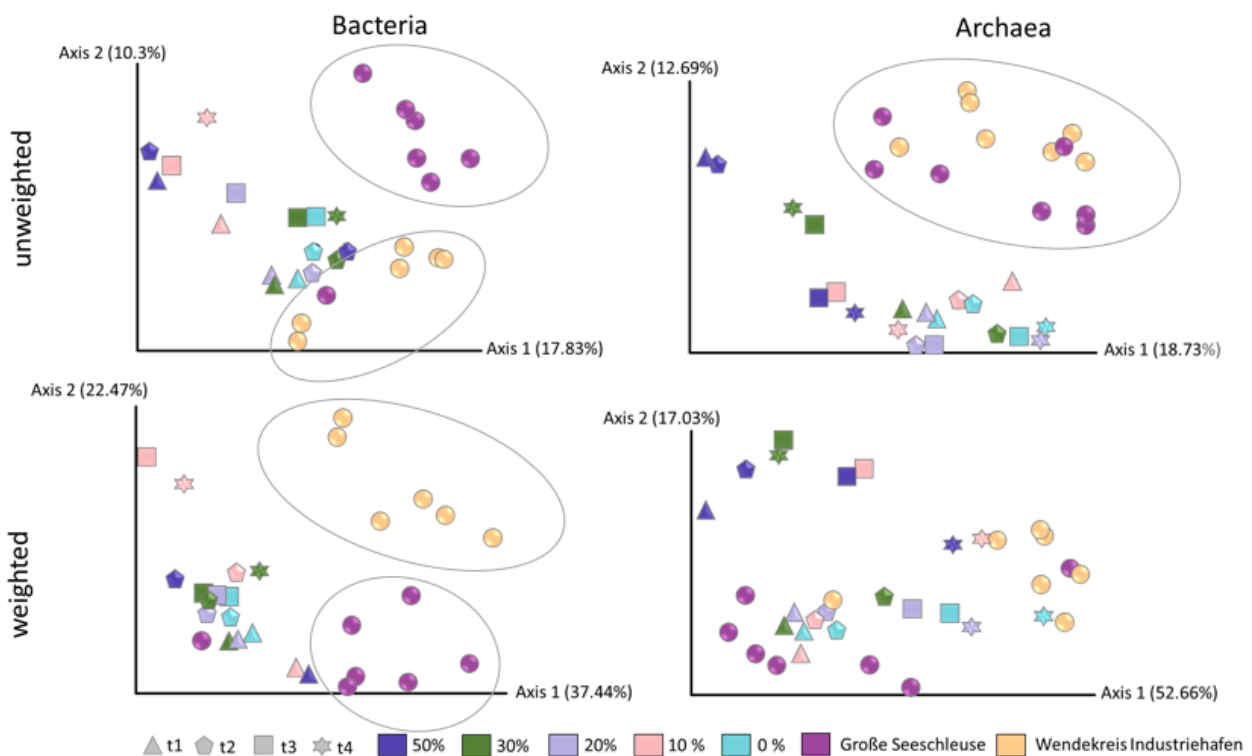
Figure 45. Intersample similarity analysis (Principal Coordinates Analysis (PCoA) plots). Weighted PCoA (top panel) includes abundance of genera, unweighted PCoA (lower panel) considers only presence or absence of genera.

4.2.3.3   Concentration and composition of extracellular polymeric substances (EPS)

The composition of EPS for all levels of substitution of saline water with freshwater were very similar and exhibited the same behavior over time (Figure 46). Towards the second sampling point (t2) an increase was observed, after which the concentration of most components steadily decreased. Over time of incubation, the concentration of total EPS excluding lipids halved in all mesocosms. In absolute terms, the acidic polysaccharides showed the strongest increase and thereafter the strongest decrease. Proteins and uronic acids remained rather stable between the first and the last sampling point, while both groups of polysaccharides were reduced to 35-41% of the original concentration. The different dynamics for the individual fractions indicate a change not only in absolute content, but also in the composition pattern over time. The temporal pattern of increase and thereafter decrease in EPS content correlates well with the degradability of organic matter, exhibiting the same dynamics (Figure 37). It is assumed that post-sampling laboratory incubation under favourable conditions of temperature in the laboratory first stimulated biomass growth and respiratory activity. As in the laboratory, no fresh biomass or easily degradable organic components were added, nor metabolites were removed, biological activity declined over time, evidenced by a decrease in EPS concentrations and changes in EPS composition.

As observed for the respiratory organic matter decay, also with respect to EPS the sample with 10% substitution of saline water with freshwater showed an exceptional behavior with acidic polysaccharides increasing to the highest concentration towards the third sampling point, but then decreasing to around the same level as in the other mesocosms. Die-off of biomass due to accidental spill of disinfectant appears to have enhanced production of acidic polysaccharides by the

heterotrophic (consumer) population, an effect that was visible until the before-last sampling point. Concentrations of acidic polysaccharides and total EPS (excluding lipids) in this sample converged to the level of the other mesocosm only by the last sampling point after 275 days.

Overall, it is seen that the effects of the long-term cut-off from the field environmental conditions, precluding for example, influx of organic matter and efflux of metabolites, had by far larger effects on the concentration an decomposition of EPS than the substitution of original water with fresh-water.
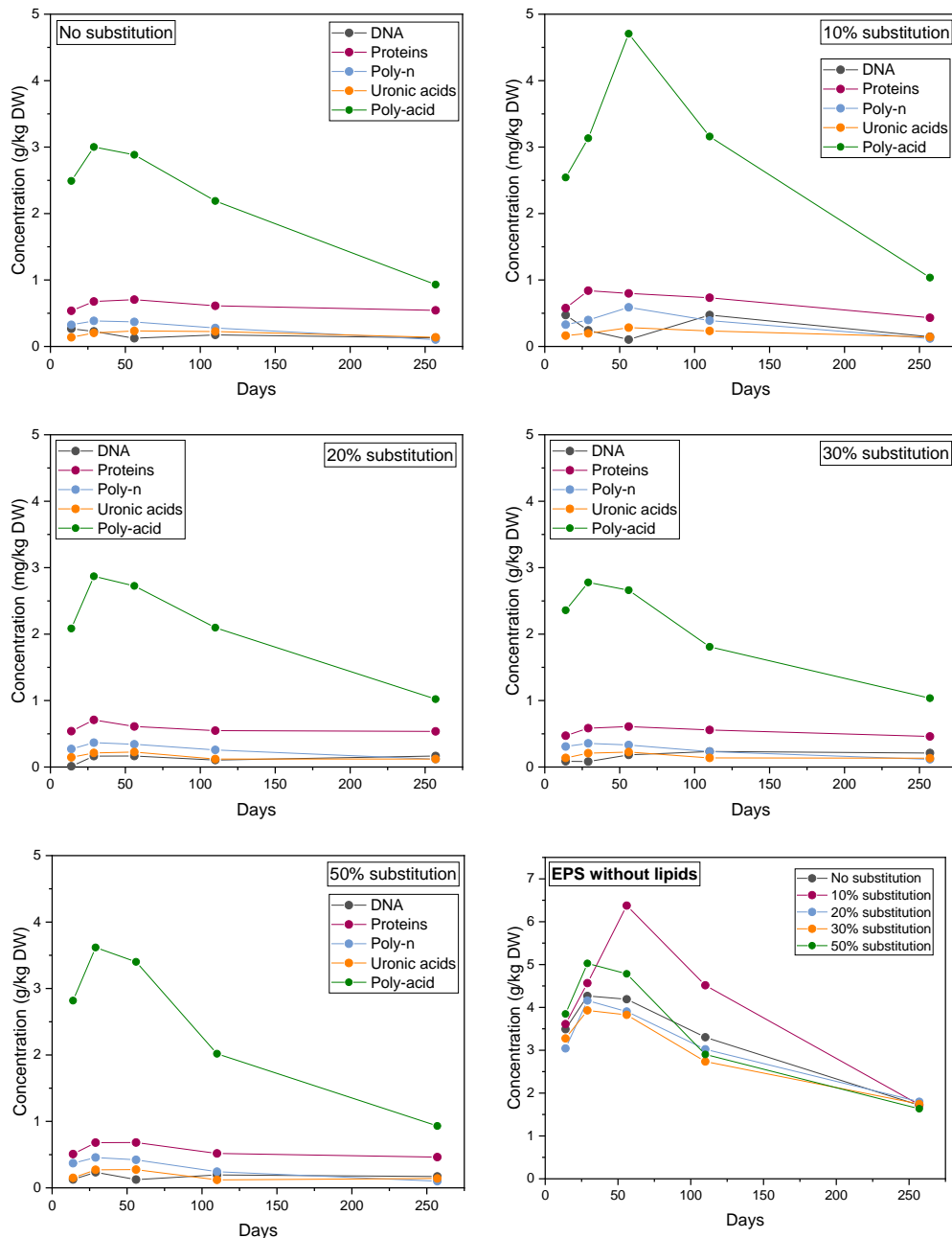
Figure 46. Change of EPS composition and total EPS concentration, excluding lipids, over time of laboratory incubation. Note that DNA concentrations are given in mg/kg DW.

4.3 Targeted laboratory experiments

4.3.1 Effect of substituting saline with fresh water on fluid mud rheology

Substitution of the fluid mud water phase with freshwater from the Ems-Jade-Kanal reduced salinity significantly, as seen from the decrease in electrical conductivity (Figure 47, left) for both samples, 1001 and 1024. However, the change in salinity had very little and no systematic effect on the yield stress (Figure 47, middle and right panel). This is attributed to the fact that the density was kept constant for all samples of the respective substitution series. Density was adjusted to the same value as the respective original, unsubstituted control sample after each freshwater admixture. It is seen that the (absent) response of yield stress to changes in salinity is similar for both samples and hence independent of the original salinity (8 mS/cm and 18 mS/cm) and original density (1.08 g/cm^3 and 1.12 g/cm^3).
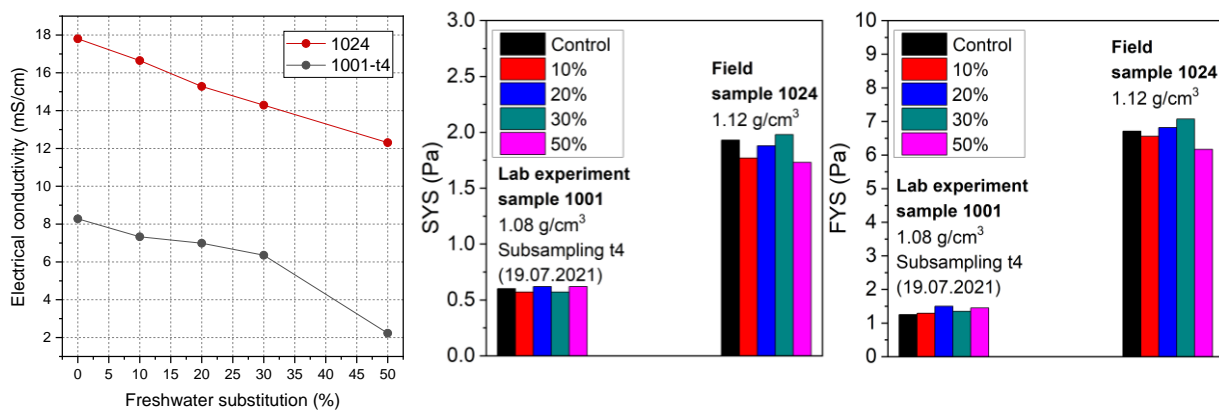
Figure 47. Effect of fresh water substitution on the electrical conductivity (EC, left), static (SYS. middle) and fluidic (FYS, right) of fluid mud samples 1001 and 1024.

4.3.2 Effect of diluting fluid mud with in situ water on settling rate and yield stress

Samples from locations sites IH and GS were diluted with in situ water to derive three samples per location that had a lower density than the original sample. As already seen for the monthly field samples (Figure 12), also in this experiment settling rates decreased non-linearly with increasing density, approaching conditions of 'hindered settling' or possibly the first phase of consolidation with a very low rate of < 5 mm/d at densities > 1.11 g/cm^3 (Figure 48, left panel). The observed trend was very similar to and is therefore considered representative of the behaviour of the field samples (Figure 48, right panel). Both SYS and FYS increased linearly with density until this threshold, higher densities result in a strong increase in slope (Figure 49).
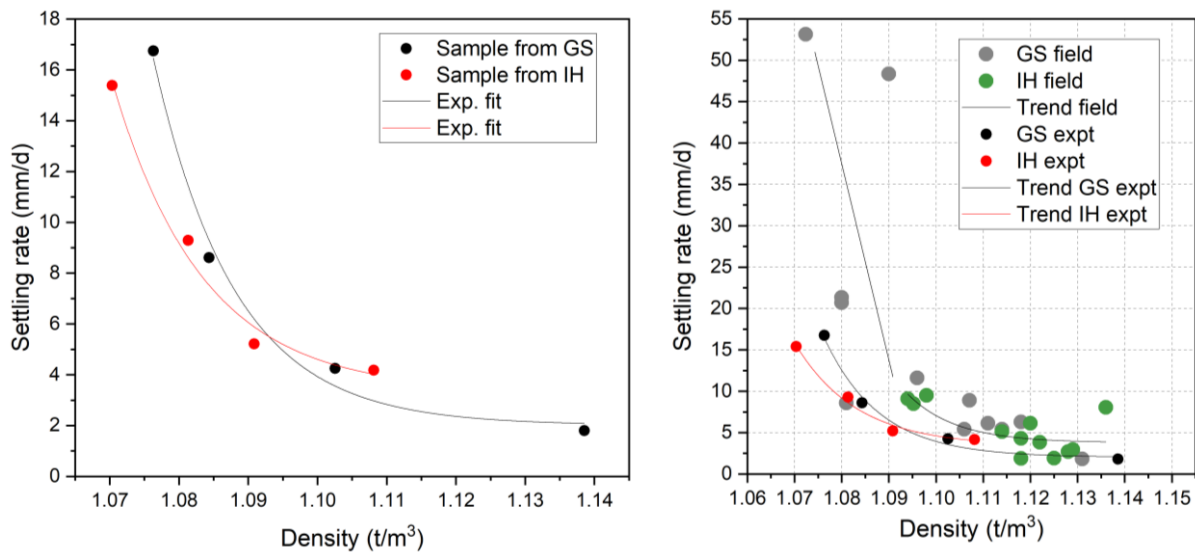
Figure 48. Relationship between density and settling rate in diluted samples from locations sites GS and IH (left) and plotted together with field data (right, see also Figure 12).
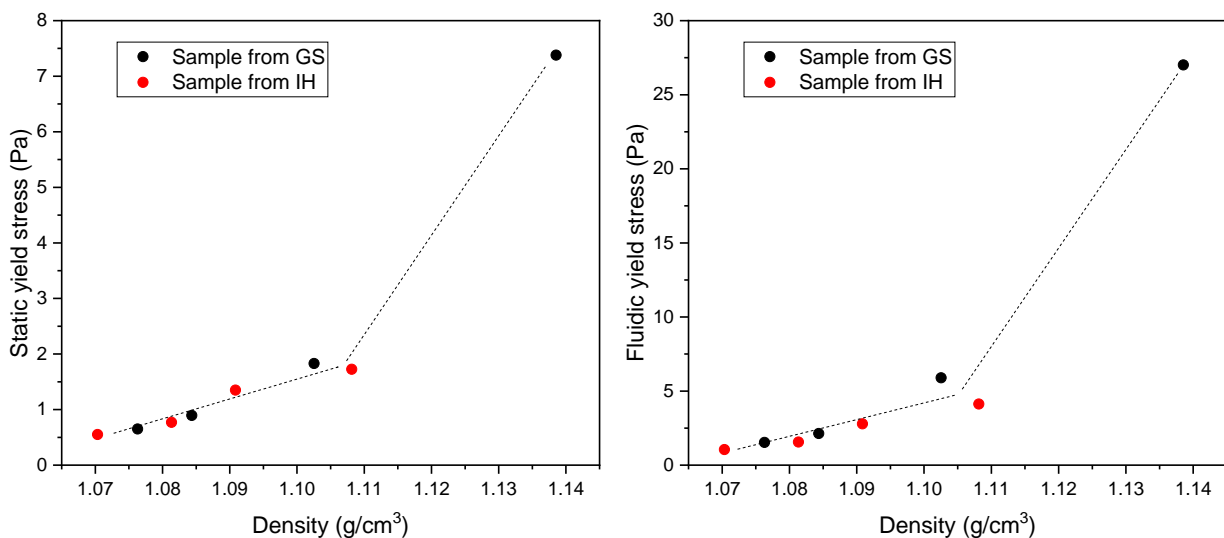
Figure 49. Relationship between density and static (SYS, left) and fluidic (FYS, right) yield stress in diluted samples 1035 from IH and 1038 from GS 1038. Dotted line serves as guidance for the observed trend.

4.3.3 Effect of diluting consolidated sediment with in situ water on mud rheology

The consolidated sediment from the non-maintained sites TB, D and B had elevated densities of 1.16 to 1.22 t/m^3 and strongly increased FYS of up to 200 Pa (Figure 50, left panel). At densities > 1.15 g/cm^3, the relationship between density and yield stresses appears to change to a much steeper slope. Upon dilution of the consolidated, dense material, however, the yield stresses aligned with the slope of each yield stress over density found for fluid mud (Figure 50, the right panel). This suggests that the low yield stresses in fluid mud from the Port of Emden are mainly density-dependent.
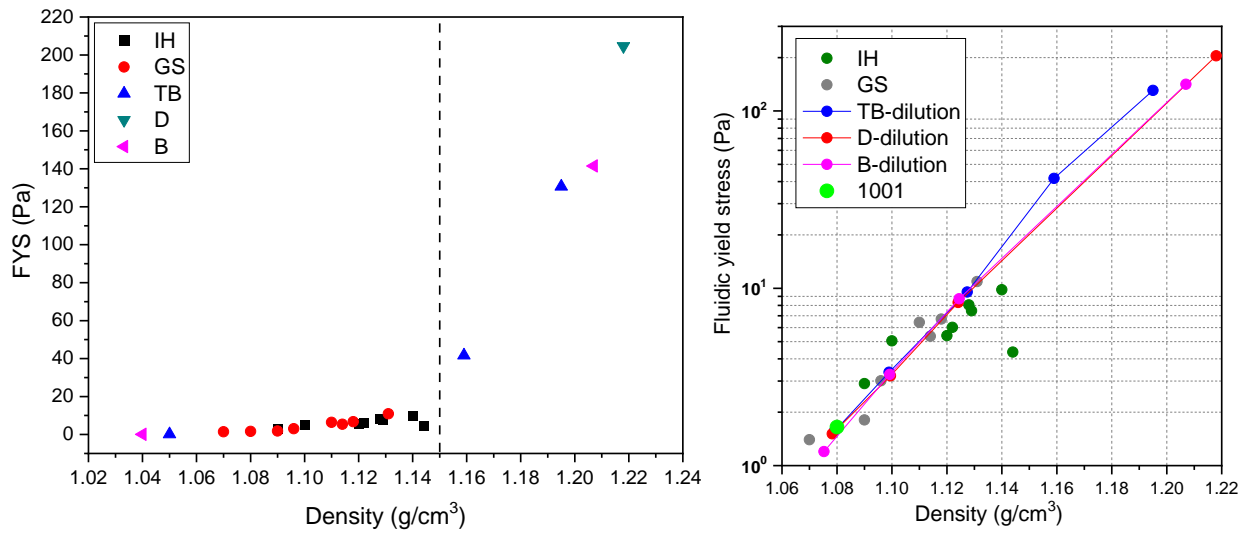
Figure 50. Relationship between density and fluidic yield stress for sites GS, IH and the non-maintained sites TB, D and B for original field samples (left) and including the diluted samples from TB,D and B (right).

5 Summary and conclusions

To assess effects of increased inflow of hinterland freshwater into the Port of Emden and of the microbial community for the efficiency of the current practice of maintenance dredging, the variability of physical, chemical and biological properties of fluid mud in the Port of Emden was investigated. The study was carried out over the period of one year by means of a field monitoring program supported by targeted experiments. Further, a laboratory study involving long-term incubation of fluid mud was used to research the effects of admixture of fresh water to the saline fluid mud.

Regarding the relationship between fluid mud properties, microbial community composition, extracellular polymeric substances (EPS), changes in the fraction of fresh water and their relevance for the effect of maintenance dredging, the following conclusions can be drawn:

- The natural, seasonal variation in the relationship between freshwater and saline water in the Port of Emden is very high. In the observation period 2021-2022, salinity varied by a factor three (~to~12 ppt) This range by far exceeds the changes predicted for the region due to climate change. Given the current maintenance practice of re-circulation dredging, no effect of the natural seasonal variation in fresh water fraction (i. e. salinity) on yield stresses and settling rates as determined on monthly field samples, could be detected.

- Yield stresses and settling rates of fluid mud in the Port of Emden are very low and are strongly density dependent. At all times, yield stresses well below 50 Pa were observed under the current practice of re-circulation dredging. The responses of yield stresses and settling rates to density can be used to define a 'window of optimum density' that allows for the desired low yield stresses in combination with low settling rates. From the results obtained in this project, densities between 1.10 and 1.15 g/cm^3 appear optimal, as they warrant low settling rates < 5-10 mm/d in combination with low shear stresses < 50 Pa.

- With respect to its chemical properties, fluid mud in the Port of Emden was characterised by high concentrations of iron (Fe), both in the solids and in the water phase. It is likely that this enhances formation of larger, open flocs which settle at low rates. Iron could either be imported by iron-rich freshwater or be released within the port from pertinent industrial activities. The source of iron and the role of the pore water composition for the flocculation behaviour should be further investigated. Redox potentials and hence oxygen saturation in the fluid mud are very low. The fact that even rigorous agitation of fluid mud with a vane, creating a substantial mixing vortex, did not significantly increase the redox potential, makes it implausible that re-circulation dredging can lead to relevant admixture of atmospheric or water phase oxygen to fluid mud. It is therefore unlikely that the microbial community is affected by enhanced oxygen availability as a result of re-circulation dredging.

- Freshwater admixture did not impact the rheological response of fluid mud, provided that the same density was maintained. This implies that future possible increases in fractions of hinterland freshwater will likely not impede the effect of the current practice of maintenance dredging. When already consolidated sediment was re-suspended with in situ water, it instantly acquired rheological properties of fluid mud, i.e. low yield stresses and the same relationship between density and yield stresses. Dilution of fluid mud further decreased the yield stresses, but increased the settling rates.

- Substituting the original water with freshwater from the Ems-Jade-Kanal did not affect the concentration nor the composition of EPS. Rather, EPS dynamics were influenced by the capped supply of easily degradable organic matter and capped efflux of metabolites as would be effective under in situ conditions. This was also supported by the well correlated dynamics in organic matter degradability, which was also unaffected by the level of freshwater admixture and showed the same temporal pattern upon laboratory incubation with a decrease following an initial increase. EPS concentrations showed a typical seasonal pattern in the field, with higher values after spring and lower values in winter, corroborating the dependency of the microbial population on net primary production. EPS concentrations are significantly lower than the ones observed for the Port of Hamburg. It therefore appears unlikely that the low density and favourable yield stress and settling behaviour result are related to EPS.

- The microbial community in field-sampled fluid mud is abundant and highly diverse. Bacteria dominate strongly over Archaea and microalgae. In contrast to sediment from the Port of Hamburg, less algae are found in fluid mud from the Port of Emden. Abundances show a temporal variation. Community composition differs distinctly between Große Seeschleuse (GS) and Industriehafen (IH) sites and the laboratory study, suggesting swift adaptation to changes in environmental boundary conditions in a material that otherwise shows very similar properties throughout the harbour area. Differences in community composition do not explain differences in organic matter degradation rates between sites GS and IH, which indicates that similar rates of substance cycling and fluxes are facilitated by different members of the community.

- Changeover to ex situ (laboratory) and substitution of saline water with freshwater both reduced relative abundance of bacteria, archaea and algae found in the original field sample. Effects initially increased with increasing level of substitution, thereafter there was no systematic pattern anymore. Also, community composition changed. Effects reflect both the capped inflow of fresh organic matter (reduced long-term cell counts) and other changes in the biogeochemical boundary conditions occurring with the change from in situ to ex-situ conditions. This was also confirmed by reduced concentrations in EPS and organic matter degradation rates. Long-term incubation levelled out the effects of different shares of fresh-water admixture, as the community in all samples adapted to the ex situ growth conditions.

Overall, the findings suggests that the low yield stresses of fluid mud in the Port of Emden are not the result of particularly high concentrations of EPS, but can be solely attributed to a reduction in density as achieved by re-circulation dredging used for port maintenance. Dredging practice could be optimised towards densities of 1.10-1.15 g/cm^3 to minimise settling rates. The diversity of the microbial community is high, its functionality redundant and it adapts swiftly to changing boundary conditions over the season, such as the strong changes in salinity or temperature. Seasonal increases in the share of hinterland water and hence the changes in environmental boundary conditions that occur already now are much larger than the changes predicted from climate change scenarios for the region. It therefore appears unlikely that increases in freshwater discharge, either due to climate change or due to changes in hinterland water management, affect the efficiency of maintenance dredging in the Port of Emden.

6 References

Adam, N., Kriete, C., Garbe-Schonberg, D., Gonnella, G., Krause, S., Schippers, A., Kurtz, S., Schwarz-Schampera, U., Han, Y.C., Indenbirken, D., and Perner, M. (2020). Microbial Community Compositions and Geochemistry of Sediments with Increasing Distance to the Hydrothermal Vent Outlet in the Kairei Field. *Geomicrobiology Journal* 37(3)**,** 242-254.

Böhnke, S., and Perner, M. (2017). Unraveling RubisCO form I and form II regulation in an uncultured organism from a deep-sea hydrothermal vent via metagenomic and mutagenesis studies. *Frontiers in Microbiology* 8(1303).

Böhnke, S., Sass, K., Gonnella, G., Diehl, A., Kleint, C., Bach, W., Zitoun, R., Koschinsky, A., Indenbirken, D., Sander, S.G., Kurtz, S., and Perner, M. (2019). Parameters governing the community structure and element turnover in Kermadec volcanic ash and hydrothermal fluids as monitored by inorganic electron donor consumption, autotrophic CO_2 fixation and 16S tags of the transcriptome in incubation experiments. *Frontiers in Microbiology* 10(2296).

Bolyen, E., Rideout, J.R., Dillon, M.R., Bokulich, N.A., Abnet, C.C., Al-Ghalith, G.A., Alexander, H., Alm, E.J., Arumugam, M., Asnicar, F., Bai, Y., Bisanz, J.E., Bittinger, K., Brejnrod, A., Brislawn, C.J., Brown, C.T., Callahan, B.J., Caraballo-Rodríguez, A.M., Chase, J., Cope, E.K., Da Silva, R., Diener, C., Dorrestein, P.C., Douglas, G.M., Durall, D.M., Duvallet, C., Edwardson, C.F., Ernst, M., Estaki, M., Fouquier, J., Gauglitz, J.M., Gibbons, S.M., Gibson, D.L., Gonzalez, A., Gorlick, K., Guo, J., Hillmann, B., Holmes, S., Holste, H., Huttenhower, C., Huttley, G.A., Janssen, S., Jarmusch, A.K., Jiang, L., Kaehler, B.D., Kang, K.B., Keefe, C.R., Keim, P., Kelley, S.T., Knights, D., Koester, I., Kosciolek, T., Kreps, J., Langille, M.G.I., Lee, J., Ley, R., Liu, Y.-X., Loftfield, E., Lozupone, C., Maher, M., Marotz, C., Martin, B.D., McDonald, D., McIver, L.J., Melnik, A.V., Metcalf, J.L., Morgan, S.C., Morton, J.T., Naimey, A.T., Navas-Molina, J.A., Nothias, L.F., Orchanian, S.B., Pearson, T., Peoples, S.L., Petras, D., Preuss, M.L., Pruesse, E., Rasmussen, L.B., Rivers, A., Robeson, M.S., Rosenthal, P., Segata, N., Shaffer, M., Shiffer, A., Sinha, R., Song, S.J., Spear, J.R., Swafford, A.D., Thompson, L.R., Torres, P.J., Trinh, P., Tripathi, A., Turnbaugh, P.J., Ul-Hasan, S., van der Hooft, J.J.J., Vargas, F., Vázquez-Baeza, Y., Vogtmann, E., von Hippel, M., Walters, W., et al. (2019). Reproducible, interactive, scalable and extensible microbiome data science using QIIME 2. *Nature Biotechnology* 37(8)**,** 852-857.

Blume, H.-P., Bruemmer, G.W., Fleige, H., Horn, R., Kandeler, E., Koegel-Knabner, I., Kretzschmar, R., Stahr, K., Wilke, B.-M. (2016). Scheffer/Schachtschabel – Soil Science. Springer. DOI 10.1007/978-3-642-30942-7.

Callahan, B.J., McMurdie, P.J., Rosen, M.J., Han, A.W., Johnson, A.J.A., and Holmes, S.P. (2016). DADA2: High-resolution sample inference from Illumina amplicon data. *Nature Methods* 13(7)**,** 581-583.

Cerqueira, T., Pinho, D., Froufe, H., Santos, R.S., Bettencourt, R., and Egas, C. (2017). Sediment microbial diversity of three deep-sea hydrothermal vents southwest of the Azores. *Microbial Ecology* 74(2)**,** 332-349.

Dellwig, O., Hinrichs, J., Hild, A., Brumsack, H.-J. (2000). Changing sedimentation in tidal flat sediments of the southern North Sea from the Holocene to the present: a geochemical approach. Journal of Sea Research 44, Issues 3–4, 195-208. DOI https://doi.org/10.1016/S1385-1101(00)00051-4.

Deng, Z., He, Q., Safar, Z., Chassagne, C. (2019). The role of algae in fine sediment flocculation: In-situ and laboratory measurements. Marine Geology 413, 71–84.

Deon, F. (2021). Report mineral investigation mud samples. Internal report TU Delft.

Ding, J., Zhang, Y., Wang, H., Jian, H., Leng, H., and Xiao, X. (2017). Microbial Community Structure of Deep-sea Hydrothermal Vents on the Ultraslow Spreading Southwest Indian Ridge. *Front Microbiol* 8**,** 1012.

Filisetti-Cozzi, T.M., Carpita, N.C. (1991). Measurement of uronic acids without interference from neutral sugars. Anal. Biochem. 197, 157-62.

Frølund, B., Palmgren, R., Keiding, K., Nielsen, P.H. (1996). Extraction of extracellular polymers from activated sludge using a cation exchange resin. Water Res. 30, 1749-1758.

Gebert, J., Zander, F., Bergmann, L., Krohn, I., Böhnke-Brandt, S., Perner, M. Linking microbial community composition, microbial biomass and extracellular polymeric substances to organic matter lability gradients in the tidal river Elbe. In preparation.

Gebert, J., Zander, F., Bergmann,L., Krohn, I., Boehnke-Brandt, S., Perner, M. Linking microbial community composition, microbial biomass and extracellular polymeric substances to organic matter lability gradients in the tidal river Elbe. Manuscript in preparation.

Gonnella, G., Böhnke, S., Indenbirken, D., Garbe-Schönberg, D., Seifert, R., Mertens, C., Kurtz, S., and Perner, M. (2016). Endemic hydrothermal vent species identified in the open ocean seed bank. *Nature Microbiology* 1(8)**,** 16086.

Hansen, C.T., Kleint, C., Böhnke, S., Klose, L., Adam-Beyer, N., Sass, K., Zitoun, R., Sander, S.G., Indenbirken, D., Dittmar, T., Koschinsky, A., and Perner, M. (2022). Impact of high Fe-concentrations on microbial community structure and dissolved organics in hydrothermal plumes: an experimental study. *Scientific Reports* 12(1)**,** 20723.

Hara, A., Radin, N.S. (1978). Lipid extraction of tissues with a low-toxicity solvent. Analytical Biochemistry 2697(78)90046-5.

Kaehler, B.D., Bokulich, N.A., McDonald, D., Knight, R., Caporaso, J.G., and Huttley, G.A. (2019). Species abundance information improves sequence taxonomy classification accuracy. *Nature Communication* 10(1)**,** 4643.

Klindworth, A., Pruesse, E., Schweer, T., Peplies, J., Quast, C., Horn, M., and Glockner, F.O. (2013). Evaluation of general 16S ribosomal RNA gene PCR primers for classical and next-generation sequencing-based diversity studies. *Nucleic Acids Research* 41(1)**,** e1.

Liefer, J.D., Garg, A., Fyfe, M.H., Irwin, A.J., Benner, I., Brown, C.M., Follows, M.J., Omta, A. W., Finkel, Z. V. (2019). The macromolecular basis of phytoplankton C:N:P uder nitrogen starvation. Frontiers in Microbiology 10:763. doi: 10.3389/fmicb.2019.00763

Liu, C., Cui, Y., Li, X., and Yao, M. (2021). microeco: an R package for data mining in microbial community ecology. *FEMS Microbiology Ecology* 26**,** fiaa255.

Luna, G. M., Manini, E., Danovaro, R. (2002). Large fraction of dead and inactive bacteria in coastal marine sediments: Comparison of protocols for determination and ecological significance. Applied and Envoronmental Microbiology 68(7), DOI: https://doi.org/10.1128/AEM.68.7.3509-3513.2002

Mietta, F., Chassagne, C., Manning, A.J.,Winterwerp, J. C. (2009). Influence of shear rate, organic matter content, pH and salinity on mud flocculation. Ocean Dynamics 59, 751-763. DOI 10.1007/s10236-009-0231-4.

Pedregosa, F., Varoquaux, G., Gramfort, A., Michel, V., Thirion, B., Grisel, O., Blondel, M., Prettenhofer, P., Weiss, R., Dubourg, V., Vanderplas, J., Passos, A., Cournapeau, D., Brucher, M., Perrot, M., and Duchesnay, E. (2011). Scikit-learn: Machine Learning in Python. *Journal of Machine Learning Research* 12**,** 2825-2830.

Price, M.N., Dehal, P.S., and Arkin, A.P. (2010). FastTree 2-approximately maximum-likelihood trees for large alignments. *PLoS One* 5(3)**,** e9490.

Quast, C., Pruesse, E., Yilmaz, P., Gerken, J., Schweer, T., Yarza, P., Peplies, J., and Glöckner, F.O. (2013). The SILVA ribosomal RNA gene database project: improved data processing and web-based tools. *Nucleic acids research* 41(Database issue)**,** D590-596.

Schippers, A., Kock, D., Höft, C., Köweker, G., Siegert, M. (2012). Quantification of microbial communities in subsurface marine sediments of the Black Sea and off Namibia. Frontiers in Microbiology 3, Article 16, https://doi.org/10.3389/fmicb.2012.00016

Shakeel A., Kirichek A., Chassagne, C. (2021). Rheology and yielding transitions in mixed kaolinite/bentonite suspensions. Applied Clay Science 211, 106206

Shakeel, A., Kirichek, A., Chassagne, C. (2020). Rheological analysis of mud from Port of Hamburg, Germany. Journal of Soils and Sediments 20, 2553-2562.

Spiekermann, J., Ahlhorn, F., Bormann, H., Kebschull, J. (2018). KLEVER: Klimaoptimiertes Entwässerungsmanagement im Verbandsgebiet Emden. Report. Accessible from https://uol.de/fileadmin/user_upload/proj/klever/KLEVER/KLEVER-Ergebnisbroschuere.pdf

Waite, D. W., Chuvochina, M., Pelikan, C., Parks, D.H., Yilmaz, P, Wagner, M., Loy, A., Naganuma, T., Nakai, R., Whitman, W.B., Hahn, M.W., Kuever, J., Hugenholtz, P. (2020). Proposal to reclassify the proteobacterial classes Deltaproteobacteria and Oligoflexia, and the phylum Thermodesulfobacteria into four phyla reflecting major functional capabilities. Int J Syst Evol Microbiol. 2020 Nov;70(11):5972-6016. doi: 10.1099/ijsem.0.004213. Epub 2020 Nov 5. PMID: 33151140.

Wingender, J., Strathmann, M., Rode, A., Leis A., Flemming, H.C. (2001). Isolation and biochemical characterization of extracellular polymeric substances from Pseudomonas aeruginosa. Methods Enzymol. 336, 302-314.

Wurpts, R., Torn, P. (2005). 15 years experience with fluid mud: Definition of the nautical bottom with rheological parameters. Terra et Aqua 99, 22-32.3

Zander, F., Groengroeft, A., Eschenbach, A., Heimovaara, T.J., Gebert, J. (2022): Organic matter pools in sediments of the tidal Elbe river. Limnologica 96, https://doi.org/10.1016/j.limno.2022.1259`97

Zander, F., Heimovaara, T., Gebert, J. (2020). Spatial variability of organic matter degradability in tidal Elbe sediments. Journal of Soils and Sediments. DOI: https://doi.org/10.1007/s11368-020-02569-4

7 Appendix

The raw data of the parameters presented in this report and further data were sent as a digital file.